Validation of a New Parametric Model for Atmospheric Correction of Thermal Infrared Data

Evan Ellicott, Eric Vermote, *Member, IEEE*, François Petitcolin, and Simon J. Hook

***Abstract*—Surface temperature is a key component for understanding energy fluxes between the Earth's surface and atmosphere. Accurate retrieval of surface temperature from satellite observations requires proper correction of the thermal channels for atmospheric emission and attenuation. Although the split-window method has offered relatively accurate measurements, this empirical approach requires *in situ* data and will only perform well if the *in situ* data are from the same surface type and similar climatology. Single channel correction reduces uncertainty inherent to the split-window method, but requires an accurate radiative transfer model and description of the atmospheric profile. Unfortunately, this method is impractical for operational correction of satellite retrievals due to the size of data sets and computation time required by radiative transfer modeling. We present a thermal parametric model based upon the MODTRAN radiative transfer code and tuned to Moderate Resolution Imaging Spectrometer (MODIS) channels. Comparison with MODTRAN showed a good performance for the parametric model and computation speeds approximately three orders of magnitude faster. Sea surface temperature (SST) calculated using atmospheric correction parameters generated from our model showed consistent results (rmse $= 0.49$ K) and small bias (-0.45 K) with the MODIS SST product (MYD28). Validation of surface temperatures derived using our model with *in situ* land and water temperature measurements exhibited accuracy (mean bias < 0.35 K) and low error (rmse < 1 K) for MODIS bands 31 and 32. Finally, an investigation of profile sources and their effect on atmospheric correction offered insight into the application of the parametric model for operational correction of MODIS thermal bands.**

***Index Terms*—Parametric modeling, remote sensing, temperature.**

I. Introduction

KNOWLEDGE of the surface temperature is critical in understanding the flux of energy between the Earth's surface and atmosphere, and therefore, a critical part of climate modeling, analyzing vegetative stress, and hydrologic modeling [1], [2]. Land surface temperature (LST) may reveal latent information about soil moisture, drought conditions, and land cover change [3]. Sea surface temperature (SST) has historically been used for meteorological and weather prediction applications, but also provides the basis for a long-term data record of climatic change [4].

Retrieval of surface temperature from spaceborne sensors has been successfully employed since the early 1980s using a variety of instruments such as the Advanced Very High Resolution Radiometer [5], [6]. Surface temperatures are typically retrieved from thermal infrared (TIR) (8–12 μm) satellite observations; however, accurate retrievals require correction for atmospheric effects. For example, attenuation of TIR satellite observations is largely due to the columnar water vapor present in the atmosphere, specifically in the lower troposphere [7]. This paper verifies the performance of a parametric model, which is tuned to the Moderate Resolution Imaging Spectrometer (MODIS), for atmospheric correction in the TIR. Ultimately, the goal is to devise a global operational atmospheric correction scheme for the MODIS sensor that would provide greater accuracy and less computational time than current atmospheric correction methods.

One particular method commonly employed for atmospheric correction of TIR data involves using the differential absorption between two spectrally discrete bands (typically at 11 and 12 μm) to account for water-vapor absorption in the atmosphere [8]. This empirical method, referred to as split window, offers a relatively accurate (± 1.0 K) method for retrieving the surface temperature, provided the surface emissivity is known explicitly or implicitly [5], [9]; implicit knowledge is obtained through the regression of satellite data to ground temperature measurements. However, this approach has several shortcomings and is subject to bias [4], [10]. The split-window approach can reliably account for atmospheric attenuation over sea surfaces where emissivity is generally well known and stable and, relying upon the empirical calibration between buoy temperature retrievals and satellite observations, achieve an accuracy of < 0.5 K [4], [5], [10]. However, there is a latitudinal, as well as hemispherical, asymmetry in the concentration of buoy temperature retrievals [11] which is a limitation to synoptic SST retrieval. In addition, bias is likely as a result of the regression process for fitting satellite-derived temperatures to buoy temperatures; in part because buoy temperatures are retrieved below the surface (bulk), while satellite radiometer-derived temperatures are based on the surface (skin) temperature [11], [12]. LST retrievals, corrected using the split-window approach, must deal with greater uncertainty in the emissivity of terrestrial features observed by satellites as a result of the heterogeneous nature of land surfaces, as well as a lack of a systematic *in situ* data available for developing the regression coefficients used in the SST algorithm. Although regionally accurate, particularly for water body targets, the split-window

Manuscript received April 10, 2007; revised September 1, 2007, February 6, 2008, and July 10, 2008. First published November 25, 2008; current version published December 17, 2008.

E. Ellicott and E. Vermote are with the Department of Geography, University of Maryland, College Park, MD 20742 USA (e-mail: ellicott@umd.edu; eric@kratmos.gsfc.nasa.gov).

F. Petitcolin is with the Analytic and Computational Research, Inc.—Earth Sciences (ACRI-ST), 06904 Sophia-Antipolis, France (e-mail: ptc@acri-st.fr).

S. J. Hook is with the Jet Propulsion Laboratory, Pasadena, CA 91109 USA (e-mail: simon.j.hook@jpl.nasa.gov).

Color versions of one or more of the figures in this paper are available online at http://ieeexplore.ieee.org.

Digital Object Identifier 10.1109/TGRS.2008.2006182

scheme is not ideal for global operational atmospheric correction of LST retrieval.

An alternative method to atmospherically correct surface temperature retrievals uses a single infrared band, typically centered at 11 μm because of limited atmospheric perturbation around this wavelength. This requires an accurate radiative transfer model (RTM) and prior information about the surface emissivity and atmospheric conditions, specifically temperature and water-vapor profiles [1], [13]. Atmospheric profiles have traditionally been retrieved from radiosonde data [14] and are often assimilated into circulation models to generate coarse, global resolution data sets, such as the National Centers for Environmental Prediction (NCEP) Global Data Analysis System ($1^\circ \times 1^\circ$, 6 h) product. A combination of atmospheric profiles with an RTM, such as MODTRAN [15], [16], provides an effective methodology to generate the corrected variables necessary for surface temperature calculation [17]. A limitation to the single channel—RTM method is the large size of data sets and, therefore, the computation time required, thus making the single channel approach generally impractical for operational correction of satellite retrievals, particularly at synoptic scales [1], [13]. Various approaches have been proposed to simplify RTM, including, but not limited to: reducing RTM to very simple equations [1], using precomputed corrections that are interpolated according to the difference between the local atmospheric profile and reference profiles [13], correlated-k model [18], or neural networks [19]. However, these approaches have their limitations. For example, [1] simplified atmospheric correction using an adjusted water-vapor continuum correction technique, achieves a processing speed $15\times$ faster than MODTRAN. The bias (1.6 K–0.8 K) in temperature retrievals using this approach, on the other hand, does not provide enough margin for accurately retrieving surface temperatures. The neural networks (NN) technique described by [19] achieved accurate results ($\text{rmse} = 0.16\ \text{K} - 0.3\ \text{K}$) and was 104 times faster than MODTRAN 3.1, but inherent limitations to neural networks were not addressed. The underlying processes are not clear, and the user may not readily have access to the underlying architecture. In addition, time is required to "train" the network (six days in the case of [19] which is fast by most NN standards). There is also an over simplification of atmospheric variables as they are integrated over the full optical path. Correlated-k models are limited when considering vertically inhomogeneous atmospheres in part because of the assumption that absorption coefficients are correlated between vertical layers.

The purpose of this study is to propose and assess the accuracy of a single channel atmospheric correction scheme which is tuned to the MODIS sensor (currently flying aboard the Earth Observing System (EOS) satellites Terra and Aqua at an altitude of 705 km, viewing the entire Earth's surface every one to two days). The goal is to achieve the same accuracy as MODTRAN, but with less computational demand by parameterizing processes used in radiative transfer modeling. Thus, the correction scheme is a tradeoff between complexity and accuracy. The parametric model was developed upon lessons learned in [17] and is based on least square fitting methodology to derive model coefficients. In [17], MODTRAN was run using NCEP profile data to retrieve the necessary atmospheric correction variables. The variables returned were then interpolated from 1° to 1 km to correct MODIS TIR observations. This was done to minimize the computation time of actually running MODTRAN using 1-km data. Since the parametric model is less computationally demanding than MODTRAN, we can now interpolate the atmospheric profile data rather than the atmospheric correction variables. This reduces the uncertainty in the correction variables which arises from the shifting view and solar angles across a 1° pixel that cannot be accounted for during the interpolation. The parametric model demonstrated a comparable accuracy to MODTRAN when testing against "reference" data sets, as well as *in situ* data. Initially, the parametric model was evaluated against MODTRAN using a synthetic data set (Sections IV and V). Sea-surface temperatures derived by the parametric model were then assessed against the MODIS SST product in Section VI. In Section VII, *in situ* lake surface and LSTs were used to investigate the model's accuracy. Finally, in Section VIII, we examined the consistency of temperature results using different combinations of available atmospheric profile data (i.e., radiosonde, satellite sounding) with the parametric model.

II. Overview of the Parametric Model for Atmospheric Corrections in TIR

Surface radiance, a variable used to calculate surface brightness temperature in the TIR, requires correction of satellite observations for atmospheric effects. Based upon top-of-atmosphere (TOA) radiance measured by spaceborne infrared sensors, upward atmospheric radiation (path radiance), downward atmospheric radiation (diffuse radiance), atmospheric transmittance, and *a priori* knowledge of surface emissivity, the following equation is generally used to retrieve surface radiance:

$$L_{\text{surf}\,\lambda} = [(L_{\text{toa}\,\lambda} - L_{\text{atm}\,\lambda\uparrow})/t_\lambda] - (1-\varepsilon_\lambda)L_{\text{atm}\,\lambda\downarrow} \quad (1)$$

where $L_{\text{surf}\,\lambda}$ is the surface radiance ($\text{W m}^{-2}\ \text{sr}^{-1}\ \mu\text{m}^{-1}$), $L_{\text{toa}\,\lambda}$ is the TOA radiance observed at the sensor ($\text{W m}^{-2}\text{sr}^{-1}\ \mu\text{m}^{-1}$), $L_{\text{atm}\,\lambda\uparrow}$ is the upwelling atmospheric radiance ($\text{W m}^{-2}\text{sr}^{-1}\ \mu\text{m}^{-1}$), $L_{\text{atm}\,\lambda\downarrow}$ is the average directional downwelling atmospheric radiance ($\text{W m}^{-2}\text{sr}^{-1}\ \mu\text{m}^{-1}$), t is the atmospheric transmittance (unitless), and ε is the surface emissivity; a dimensionless value representing the ratio of a surface's spectral radiance to a perfect black body spectral radiance, for a given temperature. An additional consideration when using satellite data is that the aforementioned equation is based on monochromatic observations while remote sensing is based on broadband observations comprised of a continuous range of wavelengths per channel (or band). Therefore, (1) will include a spectral response function (f), which is the integrated contribution of the individual wavelengths (λ) within a given band (i). The spectral integration is applied to all terms of (1) so that the surface radiance is derived from the TOA radiance, observed by the sensor in broadband.

The parametric model for atmospheric correction in TIR aims at computing the upwelling atmospheric radiance, the downwelling atmospheric radiance, and the atmospheric

transmittance, all being band integrated. Such computation requires atmospheric data along the line of sight, also known as atmospheric profile, which includes atmospheric temperature, water-vapor density, pressure, and altitude. Data provided by numerical weather prediction models such as NCEP, with 28 layers at known pressure levels between 1030 and 10 hPa, offer profiles for atmospheric correction in TIR. The proposed parametric model is based on the computation of the optical thickness τ_i $(t_i = e^{-\tau_i})$, upwelling atmospheric radiance, and the downwelling atmospheric radiance, on a layer basis, integrated along the optical path.

A. Layer Transmittance

In the TIR, layer transmission is mainly due to gaseous absorption. Molecular scattering is weak and no aerosol effects need to be considered for most cases according to Mie theory since particles are much smaller than the wavelength. The main absorbent in TIR is water vapor, for which a continuum is observed. Therefore, the optical thickness for layer l in channel i is the sum of three components for water vapor, water-vapor continuum, and other gases

$$\tau_{l,i} = \tau_{l,i}^{\mathrm{H_2O}} + \tau_{l,i}^{\mathrm{H_2Oc}} + \tau_{l,i}^{\mathrm{other}}. \tag{2}$$

The layer optical thickness of water vapor is computed using

$$\tau_{l,i}^{\mathrm{H_2O}} = \exp\left(a_{0,\mathrm{H_2O},i} + a_{1,\mathrm{H_2O},i}\rho_{\mathrm{H_2O}} + a_{2,\mathrm{H_2O},i}\rho_{\mathrm{H_2O}}^2\right) \tag{3}$$

where

$$\rho_{\mathrm{H_2O}} = \log\left(\frac{\rho_{0,\mathrm{H_2O}}}{\cos(\theta_{\mathrm{v}})}\right) \tag{4}$$

where $\rho_{0,\mathrm{H_2O}}$ is the water-vapor abundance of the layer in grams per square meter (i.e., the water-vapor density integrated along the vertical path within the layer), and θ_{v} is the view angle. The quadratic exponential form of (3) was found to be the optimal tradeoff between accuracy and simplicity. Adding terms such as $\rho_{\mathrm{H_2O}}^3$ or $\rho_{\mathrm{H_2O}}^4$ in the equation does not help capture the spectral nonlinearities of the optical thickness of water vapor within the infrared band considered. $a_{0,\mathrm{H_2O},i}$, $a_{1,\mathrm{H_2O},i}$, and $a_{2,\mathrm{H_2O},i}$ are band coefficients that depend on equivalent layer temperature (T_{l}) and equivalent layer pressure (P_{l}). The "a" coefficients are tabulated for each couple $(T_{\mathrm{l}}, P_{\mathrm{l}})$ of the atmospheric layers defined in Table I and stored in a lookup table. T_{l} (P_{l}, respectively) is computed using top layer and bottom layer temperatures (pressures, respectively), using a weighting coefficient of 0.5. Parameters $a_{0,\mathrm{H_2O}}$, $a_{1,\mathrm{H_2O}}$, and $a_{2,\mathrm{H_2O}}$ are computed using a least square fitting method for atmospheric layer configurations reported in Table I. The reference optical thickness is computed by MODTRAN for the same atmospheric layer conditions [see (9)].

For optical thickness due to the water-vapor continuum, the parametric model uses the model integrated in MODTRAN [20], [21]. The water-vapor continuum is observed absorption due to water vapor that is not attributable to the Lorentz line contribution within 25 cm^{-1} of each line. It is the difference between measured absorption and that which is predicted by theory. In other words, the continuum is absorption that cannot be accounted for by theory alone but is nonetheless real [22]. Absorption coefficients for the so-called self-broadened and foreign-broadened water-vapor continuum models have been spectrally integrated with the sensor spectral response functions. Since the spectral variations of the absorption coefficients of the water-vapor continuum are very smooth, values of $\tau^{\mathrm{H_2Oc}}$ computed by MODTRAN are reproduced by the parametric model.

TABLE I
ATMOSPHERIC LAYER CONFIGURATIONS USED FOR COMPUTING ATMOSPHERIC WATER-VAPOR LAYER DENSITY, AS WELL AS OTHER COEFFICIENTS, FROM A LEAST SQUARE FITTING METHOD

Pressure (hPa)		Air temperature range (K)			Altitude of bottom of layer (km)	Relative humidity range (%)
Bottom of layer	Top of layer	From	To	Step		
1030	1000	260	320	5	0	10, 30, 50, 70, 90
1000	975					
975	950	250	300	5	0.5	
925	900				1	
850	800	240	290	5	1.5	
750	700				2	
650	600	230	280	5	3	
550	500				4.5	
450	400	220	260	5	6	
350	300				8	
250	200	210	240	5	10	1, 10, 30, 50, 70
150	100	200	230	5	13	1, 10, 30, 50
70	50				18	1, 10, 30
30	20				24	

The layer optical thickness due to atmospheric constituents other than water vapor is computed using

$$\tau_{l,i}^{\mathrm{other}} = \exp\left(a_{0,\mathrm{other},i}\rho_{\mathrm{other}}^{a_{1,\mathrm{other}}}\right) \tag{5}$$

where

$$\rho_{\mathrm{other}} = \frac{D}{\cos(\theta_{\mathrm{v}})} \tag{6}$$

where D is the layer depth in kilometers. $a_{0,\mathrm{other},i}$ and $a_{1,\mathrm{other},i}$ are band coefficients that depend on T_{l} and P_{l}. Both parameters are derived by least square fitting over MODTRAN simulations for the layer configurations in Table I.

Finally, in order to correct for nonlinearities in optical thickness, spectral integration is applied. RTMs, such as MODTRAN, can apply the convolution with the sensor spectral response function (f) to wavelength radiances (L_λ) at layer level, as well as for the full optical path. The layer transmission is then

$$t_{l,i} = \frac{\int_{\lambda_1}^{\lambda_2} t_{l,\lambda} L_\lambda f_i(\lambda) d\lambda}{\int_{\lambda_1}^{\lambda_2} L_\lambda f_i(\lambda) d\lambda} \tag{7}$$

where the layer transmittance in wavelength λ can be decomposed as

$$t_{l,\lambda} = \exp\left(-\tau_{l,\lambda}^{\mathrm{H_2O}} - \tau_{l,\lambda}^{\mathrm{H_2Oc}}\tau_{l,\lambda}^{\mathrm{other}}\right). \tag{8}$$

However, with the parametric model, computations at numerous wavelengths are avoided in order to reduce the computation time needed for atmospheric correction. Therefore, the spectral convolution is moved to the coefficients of the parametric models that are needed to compute the layer optical thickness of water vapor, water-vapor continuum, and other gases. The spectrally integrated layer optical thickness is

$$\tau^e_{\mathrm{l},i} = \frac{\int_{\lambda_1}^{\lambda_2} \tau^e_{\mathrm{l},\lambda} f_i(\lambda) d\lambda}{\int_{\lambda_1}^{\lambda_2} f_i(\lambda) d\lambda} \tag{9}$$

with superscript e being either H_2O, H_2Oc, or other for the optical thickness of water vapor, of water-vapor continuum, and other gases, respectively. Because the exponential function is not linear and the spectral variations of the absorption coefficients of water vapor and other gases are not smooth, moving the spectral integration from radiances to optical thickness biases the layer transmissions computed with the parametric model. Such bias is corrected using a quadratic function applied to the layer optical thickness equation below, replacing the traditional $t = \exp(-\tau)$ formulation in the parametric model. The quadratic function offered the best fit while providing a tradeoff between simplicity and accuracy

$$t_{\mathrm{l},i} = \exp\left(-m_{1,l,i}\tau_{\mathrm{l},i} - m_{2,l,i}(\tau_{\mathrm{l},i})^2\right) \tag{10}$$

where m parameter is derived from least square fitting. The correction is applied to layer transmissions before they are used later in the parametric model for the computation of atmospheric upwelling radiance, atmospheric downwelling radiance, and total transmittance along the line of sight.

B. Layer Upwelling and Downwelling Radiances

Assuming the layer is a semitransparent medium in local thermodynamical equilibrium, Kirchhoff's law links the layer emission to the layer transmission so that the layer atmospheric upwelling radiance is computed using

$$L_{\mathrm{l,atm}\uparrow i} = (1 - t_{\mathrm{l},i}) L_i(T_{\mathrm{l,atm\_eq}}) \tag{11}$$

L_i is the Planck function, as introduced later in (22), convoluted with the spectral response function of band i. The equivalent layer temperature $T_{\mathrm{l,atm\_eq}}$ is derived from top layer temperature and bottom layer temperature, weighted by w (0.5)

$$T_{\mathrm{l,atm\_eq}} = wT_{\mathrm{l,bot}} + (1 - w)T_{\mathrm{l,top}} \tag{12}$$

where top and bot subscripts indicate top or bottom layer, respectively. The layer downwelling atmospheric emission integrated over the hemisphere is derived using

$$L_{\mathrm{l,atm}\downarrow i} = \left(1 - t_{\mathrm{l},i}(\theta_{\mathrm{emis}\downarrow})\right) L_i(T_{\mathrm{l,atm\_eq}}) \tag{13}$$

where $\theta_{\mathrm{emis}\downarrow}$ is the equivalent view angle for which the layer transmittance is computed to be used in the aforementioned equation. Assuming the downwelling atmospheric radiance is isotropic; [23] has shown that $\theta_{\mathrm{emis}\downarrow} = 53^\circ$ is optimal.

TABLE II
MODIS-TERRA BAND EQUIVALENT WAVELENGTHS FOR TIR BANDS

BAND	20	21	22	23	29	31	32
λ_i (μm)	3.7882	3.9921	3.9921	4.0567	8.5288	11.0186	12.0325

C. From Layer to Total Transmittance and Total Radiances

To be used in (1), total transmittance, total upwelling radiance, and total downwelling radiance along the line of sight shall be derived from layer quantities, the atmosphere being sliced in L layer with layer 1 at low altitude and layer L at top of the atmosphere. The band atmospheric transmittance t_i along the optical path is derived from the product of the transmission of the layers $(t_{\mathrm{l},i})$, yielded in (10)

$$t_i = \prod_{\mathrm{l}=l}^{L} t_{\mathrm{l},i}. \tag{14}$$

For the upwelling radiance, layer contributions are summed, accounting for the atmospheric transmittance of the layers between the layer and the sensor

$$L_{\mathrm{atm}\uparrow i} = \sum_{\mathrm{l}=1}^{L} t_{\mathrm{l}+1\to L,i} L_{\mathrm{l,atm}\uparrow i} \tag{15}$$

where $t_{\mathrm{l}+1\to L,i}$ is the transmittance along the path from top of layer l to top of the atmosphere

$$t_{\mathrm{l}+1\to L,i} = \prod_{k=l+1}^{L} t_{k,i}. \tag{16}$$

In parallel, downwelling emission reaching the surface is the sum of the layer contributions, accounting for the transmittance of the atmosphere between the layer and the surface

$$L_{\mathrm{atm}\downarrow i} = \sum_{\mathrm{l}=1}^{L} t_{1\to l-1,i}(\theta_{\mathrm{emis}\downarrow}) L_{\mathrm{l,atm}\downarrow i} \tag{17}$$

with $t_{1\to 0,i}(\theta_{\mathrm{emis}\downarrow}) = 1$.

III. ANALYSIS METRICS

The following statistics were used to evaluate the performance of the parametric model and appear, for consistency, throughout this paper. The rmse refers to the root mean square error and represents the degree of error between estimator and observed values of the quantity being investigated

$$\mathrm{rmse} = \sqrt{\frac{\sum_{i=1}^{n} (e_i - o_i)^2}{n}} \tag{18}$$

where e_{i} is the estimated value from the parametric model, o_i is the observed (or "truth"), and n is the number of observations.

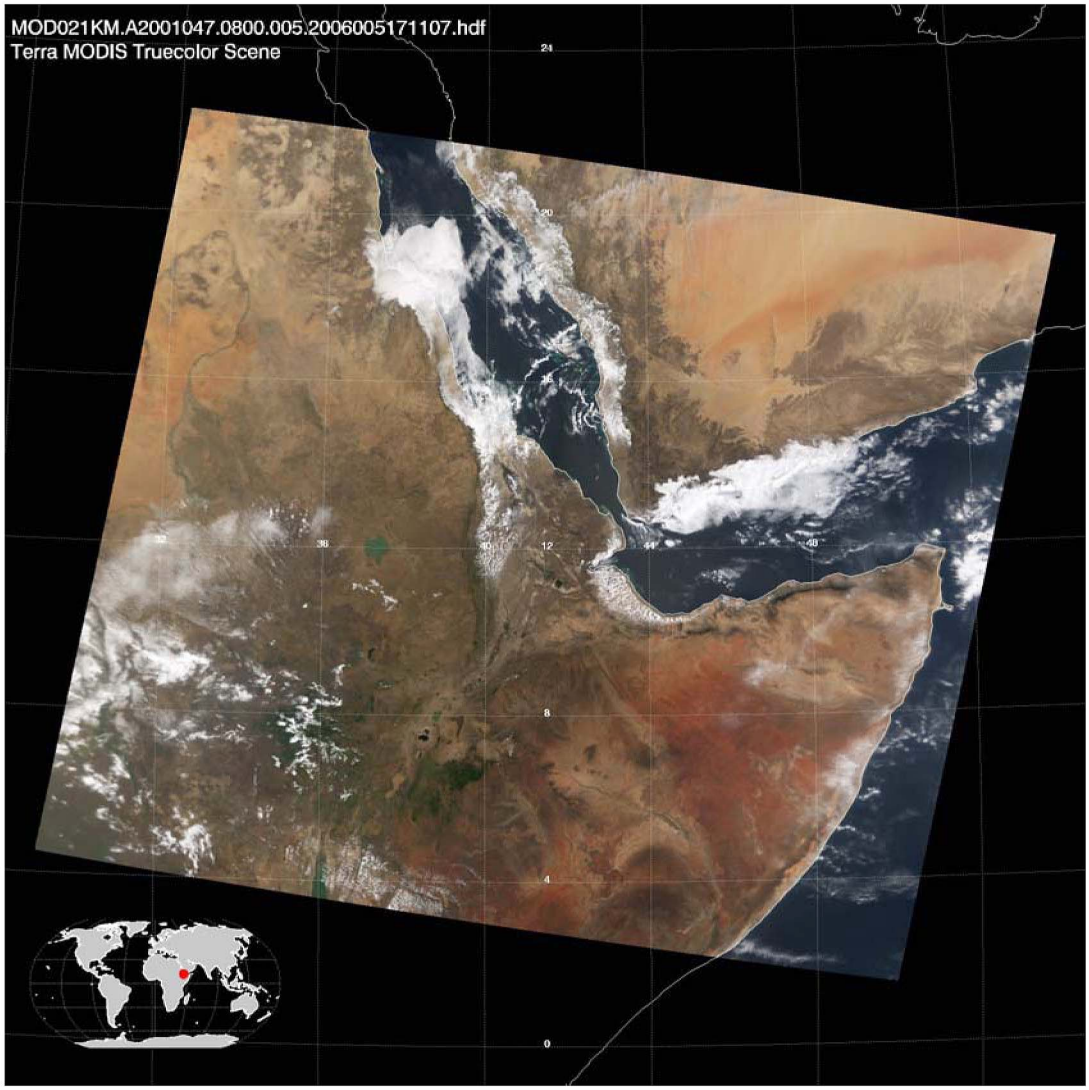

Fig. 1. Quicklook image of the Terra MODIS granule, centered at 12° N 42° E, used in the parametric model evaluation (Sections V and VI) and the subsequent results plotted in Figs. 2–7.

The mean bias provides a statistical measure of the accuracy as computed by averaged sum of differences between all estimates, e_{i} and observed (o_i) data. In our analysis, "observed" data may be a metric to evaluate the model, as in the case of comparison with MODTRAN, or actual (*in situ*) observations

$$B = \frac{\sum_{i=1}^{n} (e_i - o_i)}{n}. \tag{19}$$

Precision represents the repeatability of the estimates and is computed as the standard deviation of the estimates around the observed values, corrected for the mean bias (B)

$$P = \sqrt{\frac{\sum_{i=1}^{n} (e_i - o_i - B)^2}{n-1}}. \tag{20}$$

Finally, we use the Nash–Sutcliffe model efficiency coefficient (E) as a goodness of fit metric to assess our parametric model. In our case, we used the modified E, which replaces squaring the differences with the absolute value. This is intended to limit the bias toward extreme values

$$E = 1.0 - \frac{\sum_{i=1}^{n} |e_i - o_i|}{\sum_{i=1}^{n} |o_i - \overline{o}_i|} \tag{21}$$

where $\overline{o_i}$ is the mean of the observed values.

E ranges from $-\infty$ to 1, such that a value of $E = 1.0$ indicates a perfect match between estimated and observed values. $E = 0.0$ occurs when the model estimated values are as accurate as the mean of the observed data. While a value of $E < 0.0$ indicates that the mean of the observed values is a better predictor than the model. The motivation for using E is to provide a relative measure other than the often used coefficient of determination (R^2). According to Legates and McCabe [24], the latter is sensitive to outliers while insensitive to additive and proportional differences between the observed and predicted

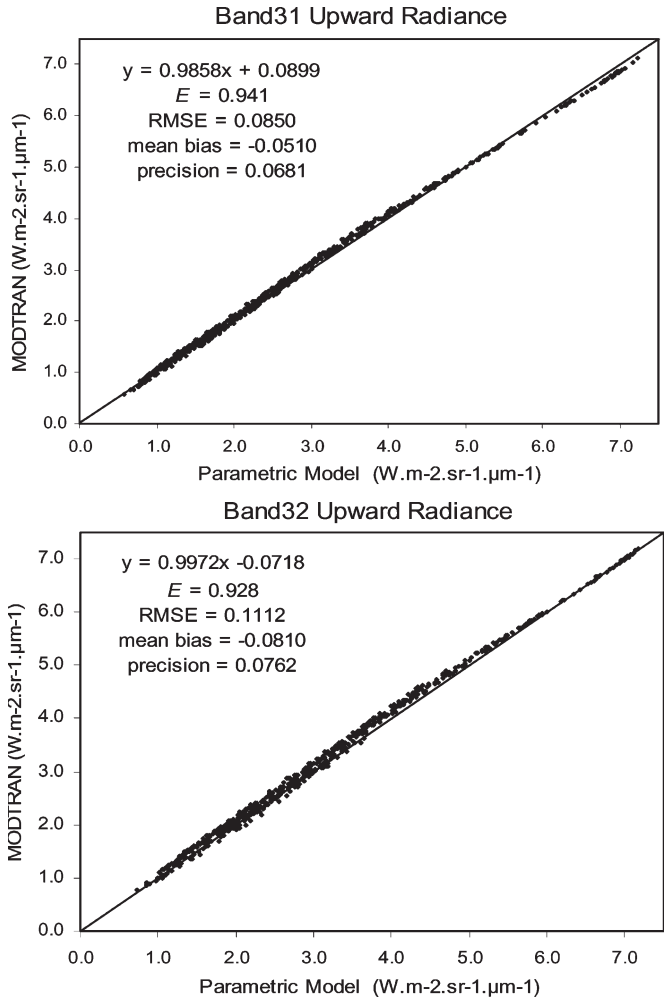

Fig. 2. Relationship between MODTRAN and the parametric model-derived upward radiance for MODIS bands 31 (11.0186 μm) and 32 (12.0325 μm). Deviation from the trend line for large upward radiances corresponds with large incidence angles and hot/moist profiles. In these cases, biases are expected due to bending of the optical path which is not accounted for in the parametric model (see Section V).

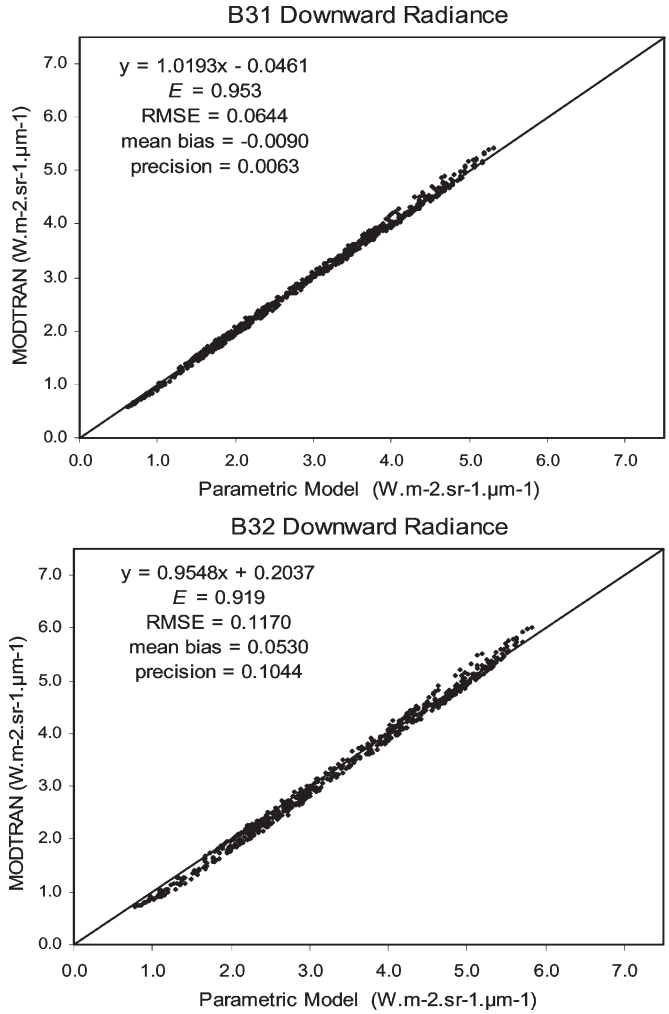

Fig. 3. Relationship between MODTRAN and the parametric model-derived downward radiance for MODIS bands 31 (11.0186 μm) and 32 (12.0325 μm). Deviation from the trend line for large upward radiances corresponds with large incidence angles and hot/moist profiles. In these cases, biases are expected due to bending of the optical path which is not accounted for in the parametric model (see Section V).

values. Thus, high values of R^2 may be achieved even when the model and observed results are quite different in magnitude.

IV. Evaluation of the Parametric Model Performance

The MODIS instrument includes seven emissive bands that are useful for surface temperature remote sensing. The additional MODIS thermal bands are designated, as an example, for atmospheric sounding and not intended for surface retrievals. Thus, initial assessment of the parameterization was based on the agreement between the retrieved parameters from MODTRAN and the parametric model in these seven bands (Table II). Evaluation of the parametric model was focused on the three atmospheric parameters derived during radiative transfer modeling ($L_{\mathrm{atm}\uparrow}$, $L_{\mathrm{atm}\downarrow}$, and t). Each data set was comprised of a MODIS granule [2004.047.0800, centered at 12° N 42° E (see Fig. 1)] and NCEP data, extracted from the work of [17], which provided geometric information related to satellite position (observation angle) and atmospheric profile data, respectively, to be used in MODTRAN and the parametric model in order to generate the aforementioned parameters. The observations had a water-vapor content range of 0.64 to 3.93 g $\cdot$ cm^{-2}; view angles between nadir and 75°; in addition, lowest layer temperature range from 286 K to 305 K. In a nominal MODIS granule, approximately 600 atmospheric profiles are available because NCEP provides profiles on a regular basis: 1° in latitude by 1° in longitude. For each of these profiles, with local observation conditions of MODIS, results of the parametric model are compared to results of MODTRAN (Figs. 2–4). Without interpolation of the atmospheric profile, both MODTRAN and the parametric model use the same atmospheric data. Therefore, the performances of the parametric model can be assessed without perturbations from atmospheric data.

A good agreement $(E = 0.9)$ was achieved between MODTRAN and the parametric model for upward radiance, downward radiance, and transmittance derived from MODIS MIR and TIR bands (Table III). Examination of the bias and precision shows the model retrievals match closely with

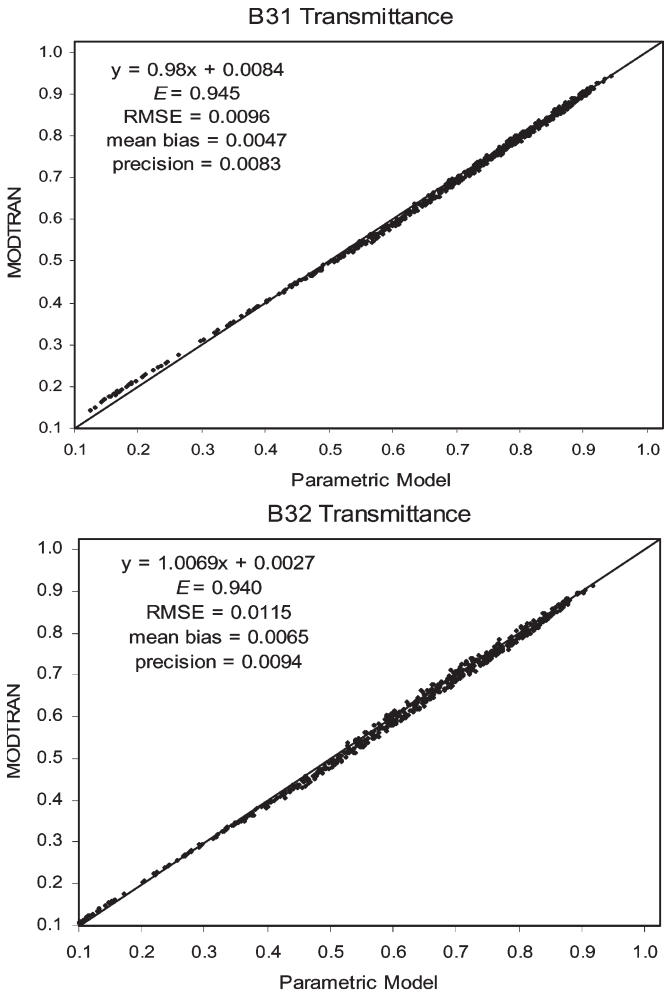

Fig. 4. Relationship between MODTRAN and the parametric model-derived transmittance.

TABLE III
PRELIMINARY EVALUATION OF RADIATIVE TRANSFER VARIABLES (a) TRANSMITTANCE, (b) UPWELLING RADIANCE, AND (c) DOWNWELLING RADIANCE WAS BASED ON COMPARISON OF THE PARAMETRIC MODEL AND MODTRAN RETRIEVALS FOR MODIS THERMAL BANDS (20–23, 29, 31, AND 32). RADIANCE VALUES ARE IN WATT PER SQUARE METER STERADIAN MICROMETER

(a)

Trans	Band	*E*	*RMSE*	*mean bias*	*precision*
MIR	20	0.8810	0.0130	0.0007	0.0034
	21	0.9880	0.0017	0.0002	0.0017
	22	0.9840	0.0019	0.0001	0.0019
	23	0.9790	0.0046	0.0021	0.0041
TIR	29	0.9110	0.0118	0.0049	0.0107
	31	0.9450	0.0096	0.0047	0.0083
	32	0.9400	0.0115	0.0065	0.0094

(b)

Up	Band	*E*	*RMSE*	*mean bias*	*precision*
MIR	20	0.8660	0.0034	0.0004	0.0034
	21	0.9850	0.0005	-0.0002	0.0005
	22	0.9680	0.0008	0.0001	0.0008
	23	0.9840	0.0008	-0.0004	0.0007
TIR	29	0.8610	0.1318	0.0735	0.1094
	31	0.9410	0.0850	-0.0510	0.0681
	32	0.9280	0.1112	-0.0810	0.0762

(c)

Down	Band	*E*	*RMSE*	*mean bias*	*precision*
MIR	20	0.6420	0.0061	0.0033	0.0084
	21	0.9260	0.0009	0.0002	0.0010
	22	0.8860	0.0012	0.0010	0.0021
	23	0.8060	0.0043	0.0029	0.0066
TIR	29	0.7470	0.2112	-0.0974	0.1876
	31	0.9530	0.0644	-0.0090	0.0663
	32	0.9190	0.1170	0.0530	0.1488

MODTRAN. Band 31 had the best agreement. This was ideal since MODIS band 31 is selectively placed, in terms of wavelength, to minimize atmospheric perturbation. On the other hand, band 29 shows the least favorable agreement between the parametric model and MODTRAN and highlights an area to improve upon the model. While Figs. 2–4 show the comparison of radiative transfer variables retrieved from the model and MODTRAN for MODIS bands 31 (11 μm) and 32 (12 μm), all of the MODIS emissive thermal bands were assessed in this section. However, particular attention was given to the two MODIS bands commonly used in surface temperature retrieval schemes; band 31 (single-channel temperature retrieval and split window) and band 32 (split window). In addition, our attention was focused on MODIS band 31 because its spectral placement was intended to minimize atmospheric perturbation and is unaffected by solar reflection during daytime observations. Thus, if the model is to prove effective, it must be accurate for MODIS band 31.

Computation speed was assessed between MODTRAN and the parametric model for retrieval of correction parameters upward radiance, downward radiance, and transmittance. Multiple trials, all conducted on the same computer (Intel Pentium 4, 2800 Hz, 512 KB cache, 1.1-GB RAM, Linux 2.4.22), showed that the parametric model was well over three orders of magnitude faster than MODTRAN. For example, for 621 profiles (approximately 28 vertical layers each) analysis of the all seven emissive bands by the model took $\sim$2 s while MODTRAN took $\sim$5800 s (Table IV). Extending this example to the estimated 288 MODIS granules produced per day highlights the significance in processing speed, particularly as it relates to operational processing. Assuming a conservative number of clear sky NCEP profiles ($\sim$300, less than half of what we typically analyzed) available from the aforementioned analysis and extending that to the 288 daily MODIS granules results in a processing time of nearly ten days for MODTRAN and less than 5 min for the parametric model. In addition, consideration must be given to the fact that preliminary analysis was performed for profiles at the NCEP resolution $(1^\circ \times 1^\circ)$ and not MODIS (1 km) in order to avoid introducing error from profile interpolation. Therefore, it can be realized that performing atmospheric correction operationally at MODIS TIR band resolution would be unrealistic with RT models such as MODTRAN but can be achieved with an accurate "fast" RTM.

TABLE IV
COMPUTATION TIME (IN SECONDS) FOR MODTRAN AND THE PARAMETRIC MODEL. COMPARISON IS BASED ON MULTIPLE RUNS OF A SINGLE GRANULE ON THE SAME MACHINE. PROGRAM EXECUTION WAS PERFORMED INDEPENDENT OF EACH OTHER (I.E., THE MODEL OR MODTRAN IS THE ONLY PROCESS RUNNING AT THE TIME ON THE MACHINE)

	time in seconds	
#	MODTRAN	PM
1	5835.42	1.52
2	5956.15	1.83
3	5798.53	2.31
4	5772.33	1.75
5	5970.44	1.89
6	5959.38	1.77
7	5802.09	1.52
8	5913.51	1.52
9	5883.26	1.52
10	5840.35	1.5
mean	5873.15	1.71

V. ASSESSMENT OF THE PARAMETRIC MODEL SURFACE BRIGHTNESS TEMPERATURE CALCULATIONS USING A SYNTHETIC DATA SET

The intention of this section was to evaluate the calculation of surface brightness temperature using realistic surface and simulated TOA radiance values, and the correction parameters generated from MODTRAN and the parametric model. Surface brightness temperature (SB(T)) was calculated for each of the NCEP atmospheric profiles introduced in the previous section. Simulated surface temperatures (T) were obtained from the temperature at the lowest atmospheric profile layer. The derivation of a realistic surface brightness temperature employed the Planck function, emissivity, and the assumed skin temperature, and was convolved with the MODIS band equivalent wavelength. The first step required calculating simulated surface radiance values

$$L_i(T_{\mathrm{surf},i}) = \varepsilon_i \frac{\frac{c_1}{\lambda_i^5}}{\exp\left(\frac{c_2}{\lambda_i T_{\mathrm{bot}}}\right) - 1} \left[\mathrm{W}\cdot\mathrm{m}^{-2}\cdot\mathrm{sr}^{-1}\cdot\mu\mathrm{m}^{-1}\right] \tag{22}$$

where c_1 and c_2 are radiation constants ($1.1911\cdot10^{-8}$ W $\cdot$ m$^{-2}\cdot$ sr$^{-1}\cdot\mu$m^4 and $1.4388\cdot10^{4}$ K $\cdot\mu$m, respectively), T_{bot} is the lowest profile layer reported temperature (here used as synthetic skin temperature), and λ_i is the MODIS band equivalent wavelength (Table II). To account for surface emissivity (ε_i), surface radiance was calculated using emissivity values typical for surfaces observed in TIR (0.98, 0.99, and 1.0). Measured at-sensor brightness temperatures were simulated using atmospheric transmittance ($\mathrm{t}_{\mathrm{mod},i}$), upward radiance ($L_{\mathrm{mod\,atm}\uparrow i}$), and downward radiance ($L_{\mathrm{mod\,atm}\downarrow i}$) computed by MODTRAN, along with the surface radiance calculated above (22), using the following formula:

$$L_i(T_{\mathrm{toa},i}) = t_{\mathrm{mod},i}\left[L_i(T_{\mathrm{surf},i}) + (1-\varepsilon_i)L_{\mathrm{mod\,atm}\downarrow i}\right] + L_{\mathrm{mod\,atm}\uparrow i}. \tag{23}$$

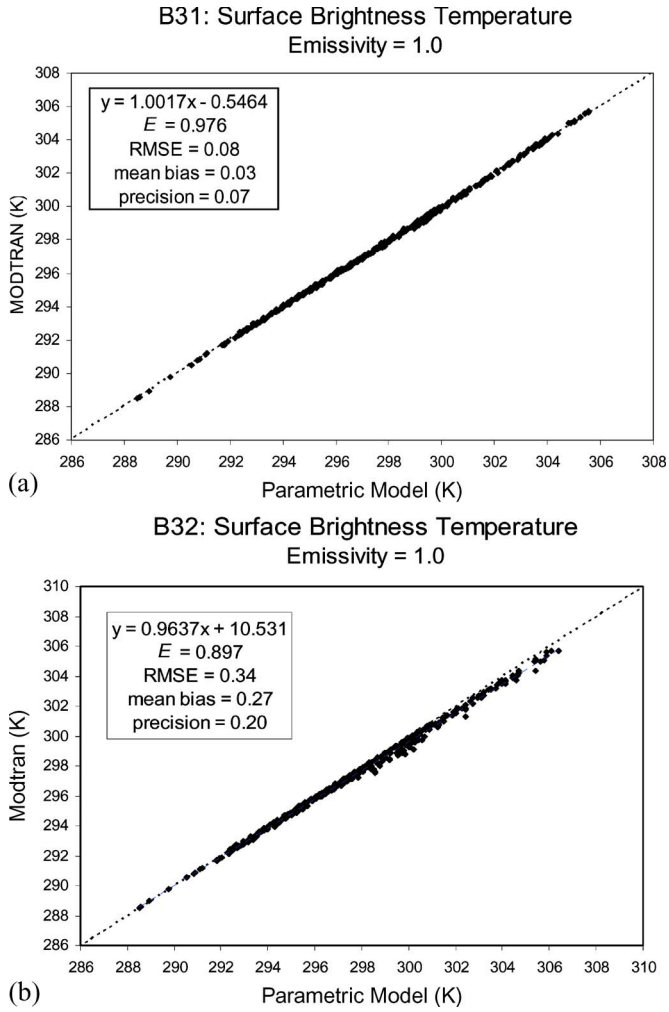

Fig. 5. Surface brightness temperatures comparison between the parametric model and MODTRAN for MODIS bands (a) 31 and (b) 32, excluding any MODIS observations with view angles greater than 60° ($n = 423$). Emissivity was set to unity. The 1:1 (dashed) line is plotted for reference.

Atmospherically corrected transmittance, upward radiance, and downward radiance values were then generated by the proposed parametric model and used along with simulated TOA radiance from (23) to calculate the surface radiance

$$L_i\left(T^*_{\mathrm{skin},i}\right) = \left[\frac{L_i(T_{\mathrm{toa},i}) - L_{\mathrm{PM\,atm}\uparrow i}}{t_{\mathrm{PM},i}} - (1-\varepsilon_i)L_{\mathrm{PM\,atm}\downarrow i}\right]/\varepsilon_i \tag{24}$$

where $L_i(T_{\mathrm{toa},i})$ is the TOA radiance from (23), $L_{\mathrm{PM\,atm}\uparrow,i}$ is the parametric model generated upward atmospheric radiance, $t_{\mathrm{PM},i}$ is the parametric model generated atmospheric transmittance, and $(1-\varepsilon)\,L_{\mathrm{atm},i\downarrow}$ is the second-order term accounting for downward atmospheric radiance.

Finally, a comparable surface skin temperature is calculated by inverting the Planck function again, this time for $L_i(T^*_{\mathrm{skin},i})$ from (24). In MODTRAN, bending of optical path is accounted for when the view angle is greater than 60°, but not in the proposed model. In such cases, the sensor does not actually "see" the surface and even small errors in atmospheric transmittance

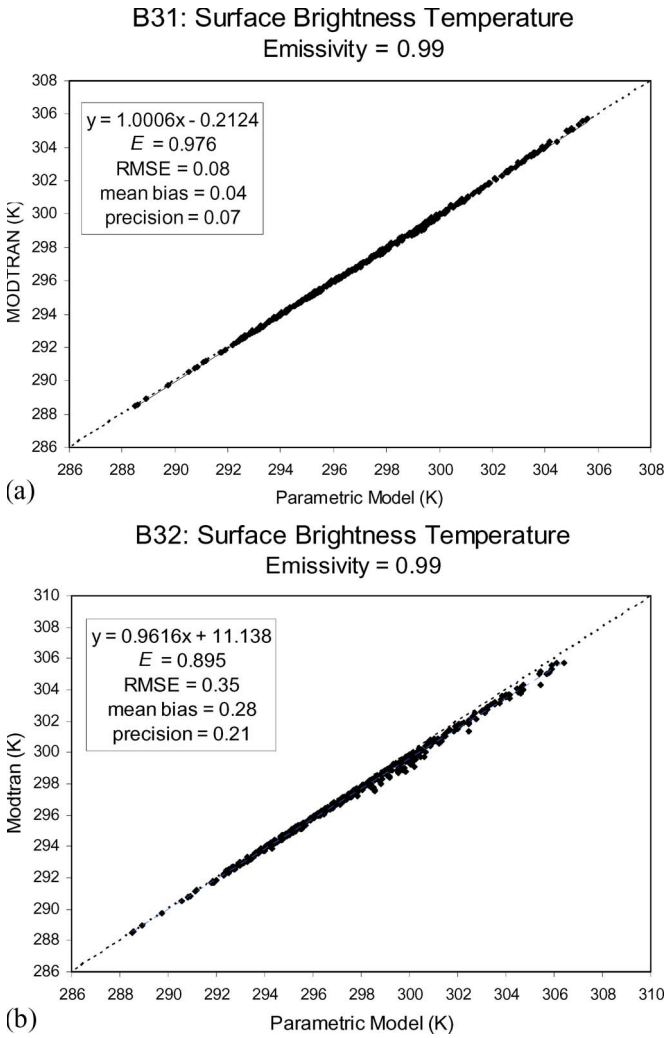

Fig. 6. Surface brightness temperatures comparison between the parametric model and MODTRAN for MODIS bands (a) 31 and (b) 32, excluding any MODIS observations with view angles greater than 60° $(n = 423)$. Emissivity was set to 0.99. The 1:1 (dashed) line is plotted for reference.

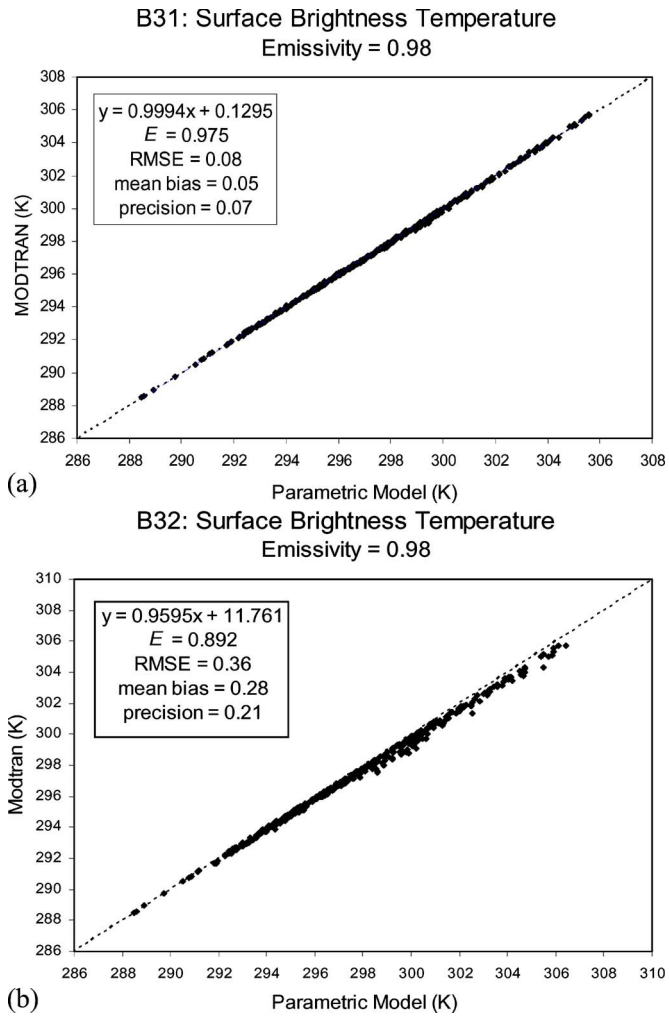

Fig. 7. Surface brightness temperatures comparison between the parametric model and MODTRAN for MODIS bands (a) 31 and (b) 32, excluding any MODIS observations with view angles greater than 60° $(n = 423)$. Emissivity was set to 0.98. The 1:1 line (dashed) is plotted for reference.

or atmospheric upward radiance have a large impact on surface brightness temperature. Therefore, we excluded observations above 60°. Fig. 5 shows a plot of the model calculated skin temperature against the synthetic skin temperatures for the MODIS granule observations in bands 31 and 32; emissivity was assumed to be unity. Additional emissivity values included 0.99 and 0.98 to represent realistic surface emission values for TIR bands 31 and 32 (Figs. 6 and 7). Table V shows the performance of the parametric model for the seven emissive bands analyzed (MODIS channel# 20–23, 29, 31, and 32). We also assessed the performance of the model when the surface temperature was assumed to be ± 5 K from the NCEP profile lowest layer temperature at each observation point. The results for this additional comparison are shown in Table VI. With exception of band 29, the results across the MIR and TIR bands examined in this paper showed a good agreement $(E \sim 0.9)$ and low error (rmse < 0.4 K) across all emissivity values. For example, the bias for band 31 was small (< 0.1 K) for the three emissivity values, while band 32 had a similar degree of bias when emissivity was unity, but increased to 0.29 K when emissivity was set to 0.98. It is clear that as emissivity decreases from unity to 0.98 that a small increase in error and bias occurs. Greater accuracy and precision is exhibited in band 31comparisons and is likely the result of the placement of this band in an atmospheric window, thus reducing the effects of water-vapor attenuation.

VI. SST Evaluation

Evaluation of the accuracy of the parametric model proceeded with a comparison of an independent measure of temperatures. Since the split-window approach is accepted to be fairly accurate over water targets (± 0.5 K [4], [5], [10]), due largely to stable emissivity, we compared the parametric model surface temperatures with the current Aqua-MODIS SST product (MYD28). Given the standard deviation in SST temperature retrievals and lacking *in situ* measurements, we used this analysis as a general comparison of temperature estimates as it is impossible to assume which is absolutely correct. The intention was to assess the consistency between the SST product and the results derived using the parametric model. The MYD28

TABLE V
STATISTICAL RESULTS FOR THE EVALUATION OF SURFACE TEMPERATURE CALCULATIONS USING THE PARAMETRIC MODEL ATMOSPHERIC CORRECTION PARAMETERS (TRANSMITTANCE, UPWARD RADIANCE, AND DOWNWARD RADIANCE). SURFACE TEMPERATURE IS ASSUMED TO BE THE SAME AS THE LOWEST LAYER OF THE NCEP PROFILE FOR EACH OBSERVATION POINT ($n = 421$). RESULTS ARE SHOWN FOR EMISSIVITY (ε) VALUES OF 1.0, 0.99, AND 0.98 AND FOR SEVEN THERMAL BANDS MODIS BANDS (20–23, 29, 31, AND 32)

ε=1.00	Band	E	RMSE	mean bias	precision
MIR	20	0.988	0.038	0.024	0.030
	21	0.995	0.014	0.012	0.007
	22	0.998	0.006	-2.5E-04	0.005
	23	0.994	0.024	-2.8E-04	0.239
TIR	29	0.684	0.879	-0.833	0.282
	31	0.976	0.080	0.034	0.073
	32	0.897	0.335	0.267	0.202

ε=0.99	Band	E	RMSE	mean bias	precision
MIR	20	0.989	0.037	0.022	0.030
	21	0.995	0.014	0.012	0.007
	22	0.998	0.006	-3.1E-04	0.005
	23	0.994	0.024	-7.6E-04	0.024
TIR	29	0.686	0.877	-0.828	0.290
	31	0.966	0.106	0.083	0.067
	32	0.895	0.346	0.277	0.208

ε=0.98	Band	E	RMSE	mean bias	precision
MIR	20	0.989	0.036	0.021	0.030
	21	0.995	0.014	0.012	0.007
	22	0.998	0.006	-3.6E-04	0.005
	23	0.994	0.024	-1.3E-04	0.024
TIR	29	0.688	0.876	-0.823	0.299
	31	0.975	0.084	0.050	0.068
	32	0.892	0.356	0.285	0.214

Level 2 product is produced daily at 1-km resolution for day and night observations and available through the Ocean Color Data Processing System (http://oceancolor.gsfc.nasa.gov). MODIS per channel radiance values were retrieved from the MYD02 (L1B) calibrated geolocated 1-km resolution product. Fig. 8 shows Quicklook images of the granules used for this comparison. This offered the necessary radiance values and view angles for the parametric model input. For atmospheric profile data, we used the MODIS atmosphere product (MYD07).[1] The MYD07 product consists of several key variables necessary for radiative transfer modeling including temperature, moisture profiles, and standard pressure levels. These parameters are recorded in 20 vertical layers. This product is also generated daily, for day and night observations, at 5-km horizontal resolution when at least nine fields of view are cloud free. The validation of sea surface temperature included 82 near-nadir Aqua-MODIS observations. The selection of near-nadir observations was intended to avoid any additional errors from angular effects. Results demonstrated a low rmse (< 0.5 K) and bias of -0.45 K (Fig. 9). The precision is 0.19 K, suggesting that the bias is systematic and consistency between temperatures exists. The accuracy and precision is encouraging, as it shows that the model agrees well on a point-to-point basis.

[1]http://modis-atmos.gsfc.nasa.gov/_docs/MOD07:MYD07_ATBD_C005.pdf.

VII. *IN SITU* VALIDATION

Ground-based surface skin temperature measurements obtained with *in situ* radiometers provided the opportunity to evaluate the accuracy of our parametric model against real surface skin temperatures that have not been derived through other modeling schemes (e.g., the SST product from MODIS). *In situ* data from two studies were used; one representing lake body targets and the other agricultural LSTs.

In the first case, observations were made over Lake Tahoe, California/Nevada, using radiometers located on four permanently moored buoys (Fig. 10) [25]. Each radiometer has been tested and calibrated to National Institute of Standards and Technology (NIST) acceptable levels corresponding with an accuracy of better than ± 0.2 K [26]. Temperatures are continually recorded at 2-min intervals, thus allowing for coincident observations with MODIS overpasses ($n = 30$). View angles ranged from 0.24° to 11.79°, while water-vapor content ranged from 0.24 to 1.94 g $\cdot$ cm^{-2}. Emissivity was obtained from the Advanced Spaceborne Thermal Emission and Reflection Radiometer (ASTER) spectral library http://speclib.jpl.nasa.gov). For a complete description of the study site, *in situ* observation methods, and results to validate satellite sensors, see [12], [27]–[29].

Validation with LST observations were made with data provided by [30]. Measurements were made with tripod mounted radiometers placed over stable, homogeneous sites in eastern Spain (Fig. 11). Accuracy of the radiometer measurements was periodically checked against a calibrated blackbody and was consistently ± 0.2 K. The box method (Rubio, 2003) was used to obtain site specific emissivity. Four radiometers were assigned to each corner of the 1-km study sites and carried along transects 100 m long to obtain a mean LST temperature. Standard deviations of averaged transect radiometer temperature measurements showed minimal variation ($\sigma < \pm 0.5$ K), and therefore, each site, as well as the study area, was assumed to be homogeneous. These ground-based LST measurements were collected within a 20- to 30-min period centered at the overpass of MODIS Terra ($n = 5$) and only temperatures measured within 3 min of the satellite overpass were used for comparison. View angles ranged from 5.47° to 27.78° and water-vapor concentration ranged from 1.35 to 2.68 g $\cdot$ cm^{-2}. A full description of the study site and methods can be found in [30].

For both comparison cases, MODIS (MYD07) profiles, retrieved at coincident observation times and locations to *in situ* temperature measurements were used in the parametric model to generate the necessary variables to derive temperatures. Emissivity values for both site surface types were retrieved from the ASTER spectral library and based on the centroid value of the spectral response function in bands 31 and 32. Lake Tahoe emissivity was set to 0.991 for band 31 and 0.985 for band 32, while the agriculture site emissivity was set to 0.984 and 0.989 for band 31 and 32, respectively. Emissivity for agricultural surface types is not explicitly available from the

TABLE VI

COMPARISON OF RMSE RESULTS FOR SEVEN THERMAL MODIS AND THREE DIFFERENT EMISSIVITY VALUES. RMSE IS BASED ON THE EVALUATION OF SURFACE TEMPERATURE CALCULATIONS USING THE PARAMETRIC MODEL-DERIVED CORRECTION PARAMETERS AND AN ASSUMED SURFACE TEMPERATURE. IN THIS TABLE, THE RMSE VALUES HIGHLIGHT THE EFFECT OF ADJUSTING THE ASSUMED SURFACE TEMPERATURE (LOWEST LAYER TEMPERATURE FROM THE NCEP PROFILES) BY EITHER ADDING (a) OR SUBTRACTING (b) 5K TO THE LOWEST LAYER TEMPERATURE AT EACH OBSERVATION POINT ($n = 421$). THE FIRST COLUMN INDICATES THE EMISSIVITY (ε) VALUE USED IN THE SURFACE TEMPERATURE CALCULATIONS. THE SECOND COLUMN INDICATES THE MODIS BAND NUMBER. THE THIRD COLUMN IS THE RMSE FOR THE ADJUSTED (± 5 K) ASSUMED SURFACE TEMPERATURE. THE FOURTH COLUMN IS THE RMSE FOR THE ORIGINAL SURFACE TEMPERATURE CALCULATIONS; AGAIN, USING THE LOWEST LAYER TEMPERATURE OF THE NCEP PROFILE AT EACH OBSERVATION POINT. THE FIFTH COLUMN DEMONSTRATES THE DIFFERENCE IN BETWEEN RMSE VALUES IN COLUMNS 3 AND 4 (ADJUSTED VERSUS ORIGINAL).

ε=1.00	Band	adj +5K	original	diff
MIR	20	0.060	0.038	-0.022
	21	0.014	0.014	0.000
	22	0.006	0.006	0.000
	23	0.024	0.024	0.000
TIR	29	0.864	0.879	0.015
	31	0.096	0.080	-0.016
	32	0.253	0.335	0.082

ε=0.99	Band	adj +5K	original	diff
MIR	20	0.058	0.037	-0.021
	21	0.014	0.014	0.000
	22	0.006	0.006	0.000
	23	0.024	0.024	0.000
TIR	29	0.861	0.877	0.016
	31	0.089	0.106	0.017
	32	0.259	0.346	0.087

ε=0.98	Band	adj +5K	original	diff
MIR	20	0.057	0.036	-0.020
	21	0.014	0.014	0.000
	22	0.006	0.006	0.001
	23	0.025	0.024	0.000
TIR	29	0.856	0.876	0.019
	31	0.083	0.084	0.001
	32	0.266	0.356	0.091

(a)

ε=1.00	Band	adj -5K	original	diff
MIR	20	0.032	0.038	0.006
	21	0.014	0.014	0.000
	22	0.009	0.006	-0.003
	23	0.024	0.024	0.000
TIR	29	0.907	0.879	-0.028
	31	0.127	0.080	-0.046
	32	0.444	0.335	-0.109

ε=0.99	Band	adj -5K	original	diff
MIR	20	0.034	0.037	0.003
	21	0.014	0.014	0.000
	22	0.010	0.006	-0.004
	23	0.024	0.024	0.000
TIR	29	0.907	0.877	-0.030
	31	0.177	0.106	-0.071
	32	0.456	0.346	-0.110

ε=0.98	Band	adj -5K	original	diff
MIR	20	0.036	0.036	0.000
	21	0.014	0.014	0.000
	22	0.010	0.006	-0.004
	23	0.025	0.024	0.000
TIR	29	0.907	0.876	-0.031
	31	0.141	0.084	-0.057
	32	0.467	0.356	-0.111

(b)

ASTER spectral library so instead we used the emissivity listed for grass. Comparison between the emissivity used by [30] of 0.985 and the emissivity values retrieved from the library show they are quite similar.

The comparison between the model and *in situ* temperature measurements shows a good agreement (MODIS band 31: $E = 0.86$, rmse $= 0.53$ K; band 32: $E = 0.78$, rmse $= 0.84$ K), with a slight systematic underestimation of the surface temperature by the model (band 31 bias $= -0.22$ K; band 32 bias $= -0.42$ K). The precision, however, shows that the standard deviation in the bias is approximately two times greater (band 31 precision $= 0.53$ K; band 32 precision $= 0.76$ K), indicating that on an individual basis, improper characterization of the atmospheric conditions and/or emissivity may exist. Fig. 12 shows the plot of the temperature retrievals between the model and *in situ* observations for band 31 and 32.

A limited number of coincident observations (30 for Lake Tahoe, 5 for Valencia) were available for *in situ* comparison and, therefore, future investigations should include more data. Nevertheless, the analysis includes a range of temperatures for two discrete surface conditions with results that are encouraging.

VIII. ATMOSPHERIC PROFILES

An important aspect of the atmospheric correction in the longwave infrared is the accuracy of the atmospheric profile used in the correction model. As part of our evaluation process, we included an additional analysis to test several sources of atmospheric data with the idea that an operational atmospheric correction scheme for MODIS could be developed using our parametric model and an accurate profile retrieved via coincident satellite sounding. Three sources of atmospheric profile data were compared; the Integrated Global Radiosonde Archive (IGRA), positioned as our reference data since *in situ* measurements are made along the path of ascent in the atmosphere; MODIS profile retrieval product (MYD07), discussed earlier; and the Atmospheric InfraRed Sounder (AIRS).[2]

The IGRA[3] database [14] consists of 1500 globally distributed sounding stations with data records spanning over 30 years. Generally, each station makes two daily launches at

[2]http://eospso.gsfc.nasa.gov/eos_homepage/for_scientists/atbd/docs/AIRS/AIRS_L1B_ATBD_Part_1.pdf.

[3]http://www.ncdc.noaa.gov/oa/cab/igra/index.php.

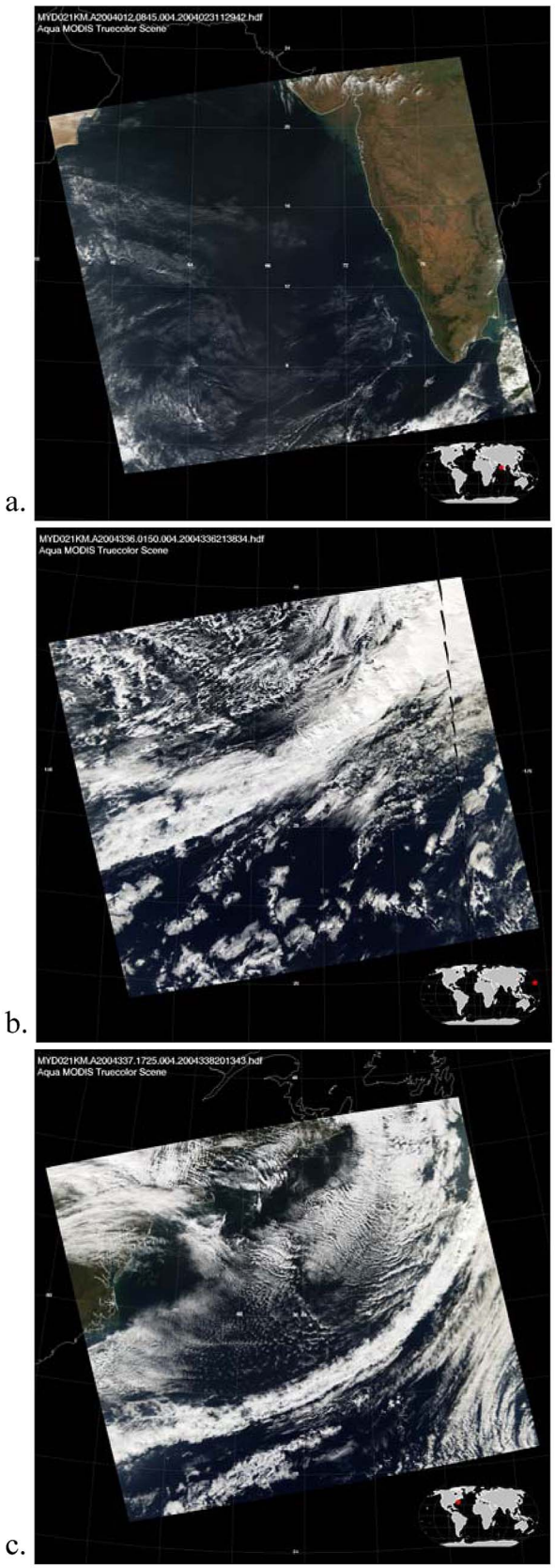

Fig. 8. Quicklook images of the Aqua MODIS granules used in the SST comparison section (Section V) and the results plot (Fig. 9). (a) Granule 2004.012.0645 centered at 14° N 70° E. (b) Granule 2004.336.0150 centered at 30° N 170° E. (c) Granule 2004.337.1725 centered at 36° N 64° W. Granule nomenclature indicates year.doy.hhmm, where doy is the day of year, and hhmm is the time in hours-minutes (UTC).

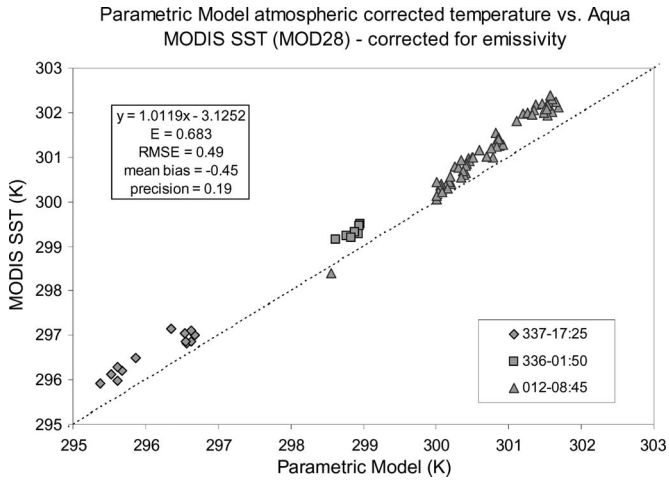

Fig. 9. Comparison of the atmospherically corrected sea surface temperatures using the parametric model (MODIS band 31) versus the Aqua-MODIS sea-surface temperature product (MYD28). Since emissivity correction is performed for the MODIS SST product, we accounted for emissivity as well when deriving surface temperatures with the parametric model. An emissivity of 0.995 was assumed; generally accepted as a standard sea surface emissivity for MODIS band 31. Near-nadir observations are from 2004 $(n = 78)$ with diamonds corresponding with day of year (DOY) 337 at 17:25 UTC; squares with DOY $= 336$ at 01:50 UTC; and triangles with DOY $= 012$ at 08:45 UTC. The 1:1 (dashed) line is plotted for reference.

1100 and 2300 UTC. Profile observations are provided at standard, surface, tropopause, and significant levels. Standard level variables include pressure, temperature, geopotential height, dew point temperature, wind direction, and wind speed. The standard level product generally had a vertical resolution of 20 layers. We expanded the vertical resolution of the standard level product by including variables from the significant thermodynamic layer product, therefore creating a profile that included approximately 40 vertical layers. We assumed the radiosonde profiles to be the benchmark by which to compare other profiles. Since NCEP profiles are assimilated products incorporating radiosonde data, we chose not to replicate analysis with this data. Rather, the intention is to view the radiosonde data as a potential source of data to act as a "truthing" product to validate the satellite-derived profiles, much in the way that the Aerosol Robotic Network (AERONET)[4] system is used for aerosol retrievals. We found, however, that many radiosonde launch stations recorded sporadic or incomplete profile information which may limit the functionality as a global validation data set. In some cases, the data were completely missing for a given satellite overpass or the vertical content was too small to be useful (e.g., < 10 layers).

AIRS is a high spectral resolution spectrometer with 2378 channels in the TIR, ranging from 3.7 to 15.4 μm. The standard product provides global, twice daily coverage at 50-km horizontal and 28 layer vertical resolutions for any given location; the vertical resolution was interpolated to 40 layers to match the radiosonde profiles for consistency. Among the variables recorded, the most relevant includes geopotential surface and layer height, water-vapor mixing ratio, water-vapor saturation mixing ratio, surface and layer temperature, standard pressure

[4]http://aeronet.gsfc.nasa.gov/F_Info/system_info_additional.html.

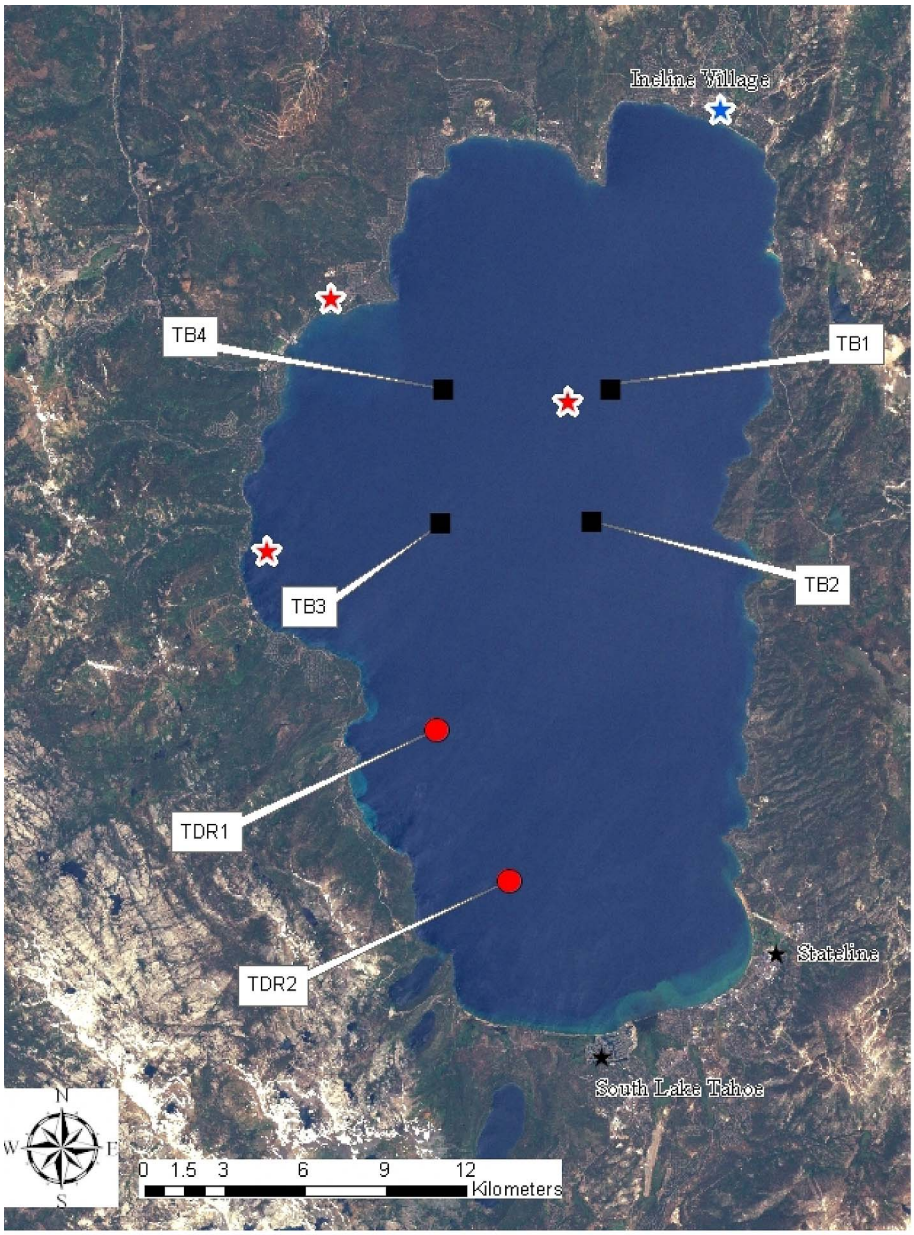

Fig. 10. Lake Tahoe, California/Nevada showing the four National Aeronautics and Space Agency buoys labeled as TB1, TB2, TB3, and TB4 (Tahoe Buoy #). Water properties are measured at the Midlake (star near TB1) and the Index station (star west of TB3). Meteorological measurements have been made at both Incline (blue star) and the USCG site (red stars northwest of TB4). University of California at Davis also maintains two additional floats (rafts) in the southern part of Lake Tahoe (TDR1 and TDR2) which measure meteorological variables and bulk temperature. South Lake Tahoe and Stateline towns are shown for reference (black stars).

levels, columnar water vapor, and quality flags. Since the AIRS sensor is aboard Aqua, it provides temporally coincident observations with MODIS, but at higher spectral resolution and greater profile sounding vertical resolution. However, the spatial resolution of AIRS (50 km) is nearly 50 times coarser than MODIS radiance retrievals (1 km), and ten times coarser than the MYD07 product (5 km).

It should be stated that we assume near coincident observations. Although it is unrealistic to think that the timing and, therefore, the profiles retrieved from the three sources will be identical, this analysis offered an opportunity to investigate several sources of profile data to see how closely the temperatures, produced using at-sensor radiances, corresponded.

MODIS L1B radiance retrievals were once again used as the TOA observation data to be adjusted for atmospheric perturbations. Incorporating the radiosonde profiles into MODTRAN returned the necessary correction parameters which were then used to calculate synthetic "reference" surface brightness temperatures to compare with the parametric model. For comparison, the two satellite-derived atmospheric profile products available aboard the Aqua satellite (AIRS and MODIS) were used with the parametric model to correct TOA radiances and calculate surface temperatures. Coincident observations between Aqua and radiosonde soundings were limited to the launch times of at IGRA stations. We also chose stations that offered coastal launches and prevailing winds that would

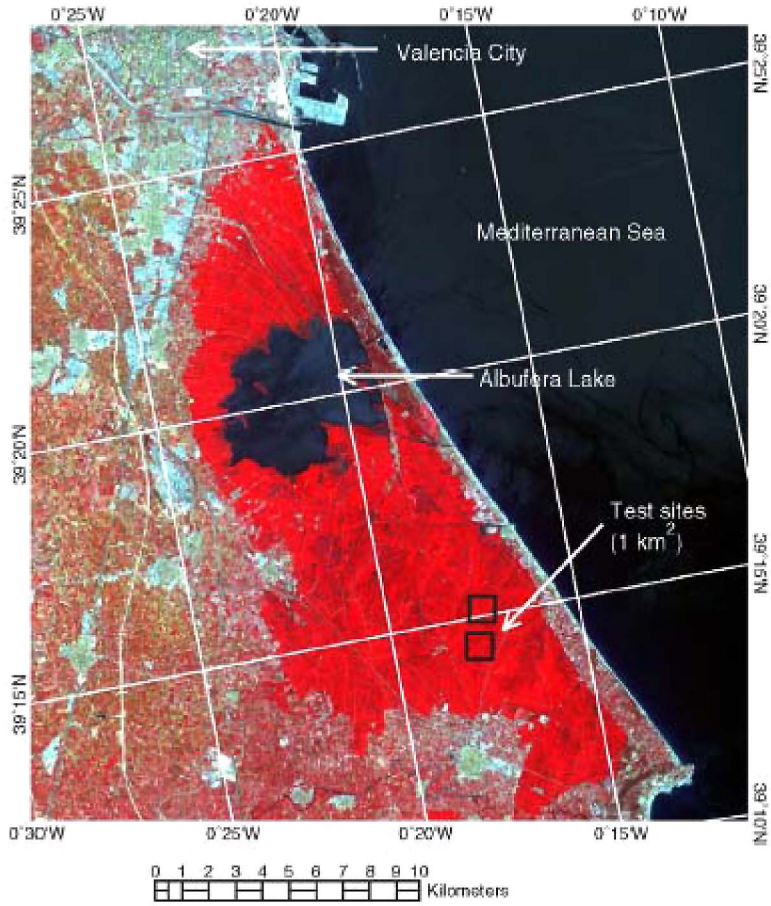

Fig. 11. Study sites used for measurement of LST. *In situ* data were recorded along transects within flat homogeneous plots consisting of cultivated rice fields. The above image is an ASTER color composite ($R = 0.81\ \mu$m; $G = 0.66\ \mu$m; $B = 0.56\ \mu$m) from August, 2004. Courtesy of César Coll.

provide open water observations, reducing emissivity uncertainty, and allowing for comparison with AIRS and MODIS. Several locations in the Mediterranean Sea were chosen for their ideal physical location and coincidence of Aqua satellite overpass with radiosonde launch.

Fig. 13 shows the agreement between the "reference" temperatures and the AIRS-parametric model-derived temperatures for MODIS bands 31 ($E = 0.88, \text{bias} = -0.02\ ^\circ\text{C}$) and 32 ($E = 0.84, \text{bias} = -0.04\ ^\circ\text{C}$). The rmse for both bands indicates the error in the match between the temperature derivations is less than 1 K. The precision indicates, however, that on a point-by-point basis, the temperatures deviate by an average of 0.5 K and 0.8 K for band 31 and 32, respectively. A limited number of observations ($n = 15$) and an average difference of 0.44 $\text{g} \cdot \text{cm}^{-2}$ in the water-vapor content recorded by the radiosonde and AIRS may be the cause.

The corresponding comparison between the radiosonde-MODTRAN reference temperatures and the MYD07-parametric model temperatures showed less agreement for bands 31 ($E = 0.50$) and 32 ($E = 0.13$) than the AIRS-parametric model temperature comparisons above. Residual error and bias were greater as well (band 31 rmse $= 1.50$ K, bias $= 1.26$ K; band 32 rmse $= 2.61$ K, bias $= 2.21$ K) (Fig. 14). The precision shows that the spread of data does not agree well either. The larger bias generated when using the MODIS profile data may be in part due to lower spectral resolution as compared with AIRS. In addition, the mean difference in water-vapor content between MODIS and the radiosonde retrievals was 2.7 $\text{g} \cdot \text{cm}^{-2}$, significantly greater than between AIRS and radiosonde retrievals. Indeed, validation of MOD07 product for the most recent reprocessing ("Collection 5") demonstrated greater bias by the MODIS product than AIRS when evaluated against best estimate profiles taken from radiosonde retrievals.[5]

The consistency between the radiosonde-MODTRAN reference temperatures and parametric model-AIRS calculated temperatures offered promising results. Conversely, the parametric model-MOD07 temperatures did not match well with our "reference" temperatures, but provided clear evidence for the necessity in obtaining accurate atmospheric data. For example, coincident temporal retrievals of TOA radiance and atmospheric conditions from satellite retrieval reduce uncertainty introduced from the interpolation of radiosonde measurements. On the other hand, radiosonde measurements offer *in situ* information about the atmospheric conditions through direct sampling, and clearly interpolation (spatial and temporal) of radiosonde measurements is necessary

[5]http://modis-atmos.gsfc.nasa.gov/_docs/MOD07:MYD07_ATBD_C005.pdf.

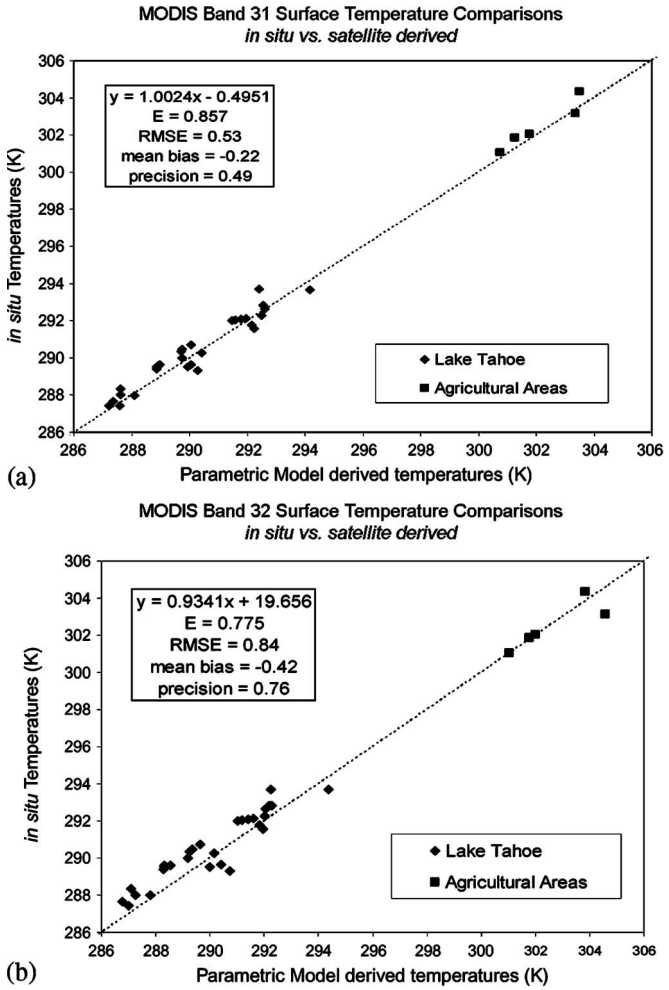

Fig. 12. Comparison of surface temperatures derived from *in situ* radiometric measurements versus the parametric model-derived temperatures for (a) band 31, and (b) band 32. Emissivity values used for the model calculated temperatures were retrieved from the ASTER spectral library. For Lake Tahoe, represented by the blue diamonds, was set to 0.991 and 0.985, while emissivity for the agricultural site was 0.984 and 0.989 (band 31 and 32, respectively). The MODIS atmosphere product (MOD07) was used for the atmospheric profile input data in the parametric model. The 1:1 line (dashed) is shown for reference.

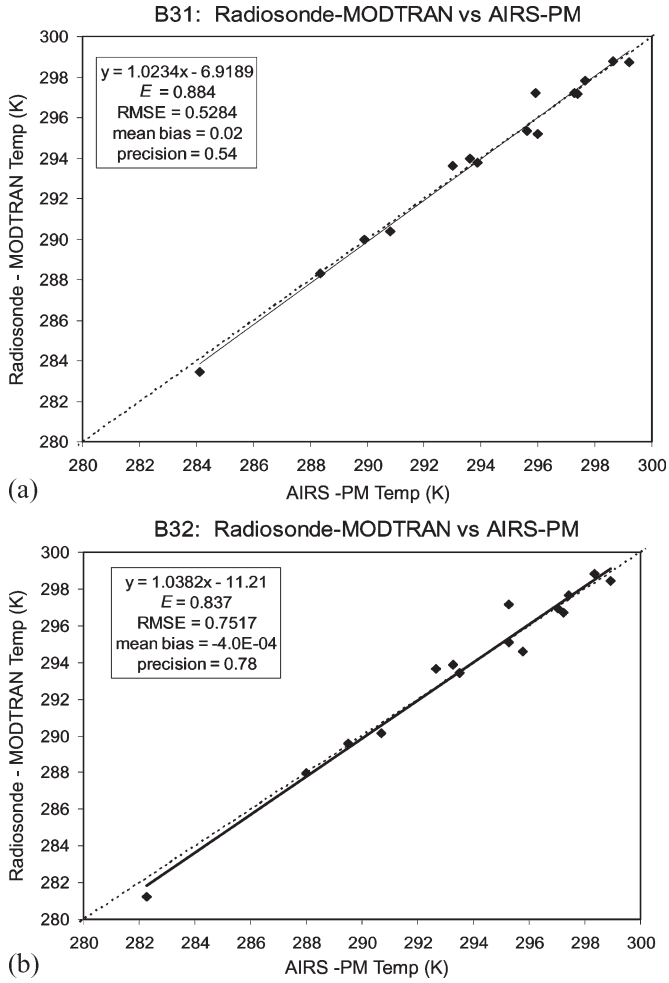

Fig. 13. Comparison of calculated sea surface temperatures. Radiosonde profiles used in MODTRAN offer "reference" temperatures to compare the AIRS profile—parametric model-derived temperature estimates. MODIS band (a) 31 and (b) 32. The 1:1 line (dashed) is shown for reference.

for atmospheric data to be used on a global operational scale. Frequent and regular validation of the MODIS and AIRS profiles against radiosonde measurements would insure product accuracy and offer a quantitative measure of uncertainty in the products. Another consideration is the vertical resolution of soundings which influences the accuracy of RTM estimates. The advantage AIRS offers over MODIS is greater vertical detail of the atmosphere, but this is offset by the lower horizontal resolution. Something of a combination between the MODIS horizontal and AIRS vertical resolutions would offer greater detail about the true atmospheric conditions.

IX. Summary and Conclusion

The purpose of this paper was to propose and assess the accuracy of a single channel atmospheric correction scheme which is tuned to MODIS and achieve the same accuracy as MODTRAN with less computational demand. The parametric model offers an approach to operationally correct the at-sensor radiance values for atmospheric perturbations. Evaluation of the parametric model against MODTRAN showed consistent results for retrieval of correction parameters. For example, the mean bias for all seven bands analyzed for transmittance was $=$ 0.0027 with a mean precision was 0.0056. The improvement in computation speed to calculate the correction parameters was over three orders of magnitude faster than MODTRAN ($\sim$2 s versus $\sim$5800 s, respectively). This is a significant increase when considering the enormity of performing such computations on a global operational basis. Comparison of surface temperatures calculated using the parametric model against the MODIS SST (MYD28) showed a good agreement (rmse $=$ 0.49 K) with individual point retrievals within -0.45 K $\pm$ 0.19 K of the MODIS estimates. It should be reiterated that we do not assume the MYD28 product to be a surrogate for *in situ* measurements. Rather, our comparison was intended to assess if the parametric model is consistent with an estimate that is a standard MODIS product.

Evaluation of MODIS surface temperature retrievals, corrected for atmospheric effects with the parametric model, versus *in situ* temperature retrievals demonstrated the model's

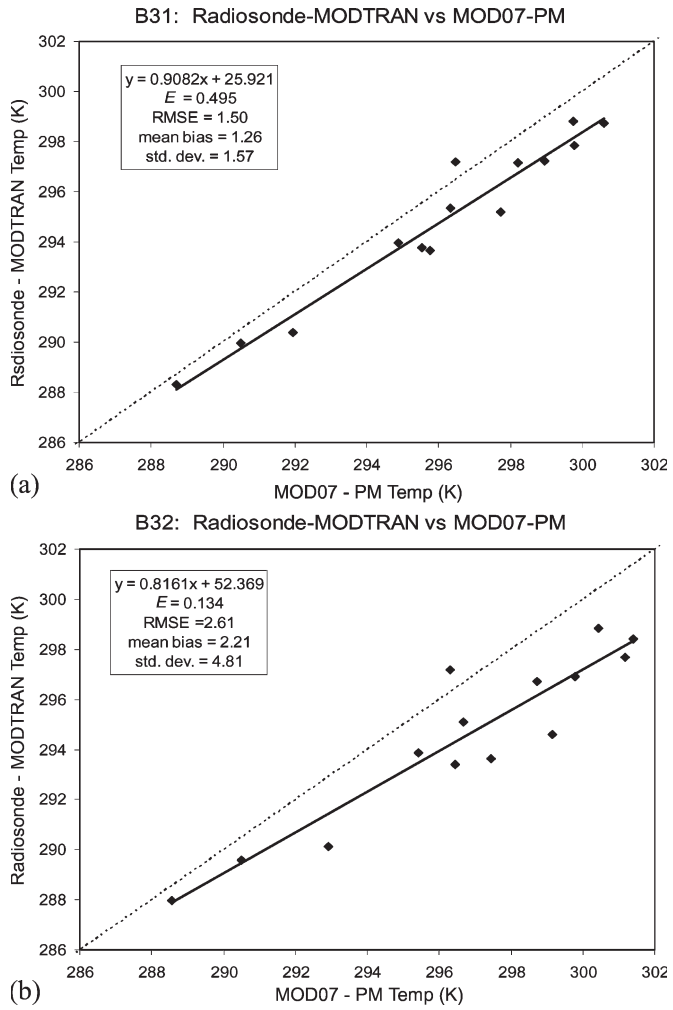

Fig. 14. MODIS (a) band 31 and (b) band 32 comparison between the radiosonde-MODTRAN "reference" surface temperatures and MOD07—parametric model-derived temperatures. The 1:1 line (dashed) is shown for reference.

ability to accurately retrieve correction parameters. For band 31, and both surface types (LST and SST), the bias was -0.22 K with an rmse of 0.53 K, while for band 32, the bias was -0.42 K with an rmse of 0.84 K. This is well within the reported LST accuracy of 1 K reported by [31]. The precision for both bands was roughly a factor of two greater (0.49 K and 0.76 K, band 31 and 32, respectively) indicating variability between retrievals, perhaps due to some heterogeneity in the surface conditions.

Consideration of the profiles used in radiative transfer modeling is paramount to achieving accurate correction for atmospheric effects. This paper touched on a few sources of satellite profile data and demonstrated their relatively accuracy when compared with radiosonde atmospheric retrievals. However, nonuniformity of atmospheric water vapor between profile sources suggests that obtaining a profile that accurately reflects the true atmospheric state may be difficult. Consistent periodic sampling to validate profiles, similar to the current aerosol—AERONET framework used for the MODIS aerosol product, should be developed. Although it was our hope that radiosonde data could provide the basis for site specific validation data, our research has shown that inconsistency in radiosonde launch timing and profile retrieval at some sites limits the effectiveness of this data source for synoptic vicarious calibration. Nevertheless, a focus on developing an operational scheme for near-real time atmospheric correction of MODIS MIR and TIR bands using profile data retrieved from AIRS and MODIS should be considered; MODIS providing the spatial resolution and AIRS providing the necessary accuracy.

ACKNOWLEDGMENT

The research described in this paper was carried out in part at the Jet Propulsion Laboratory, California Institute of Technology, under a contract with the National Aeronautics and Space Administration. Reference herein to any specific commercial product, process, or service by trade names, trademark, and manufacturer or otherwise does not imply endorsement by the United States or the Jet Propulsion Laboratory, California Institute of Technology.

REFERENCES

[1] A. N. French, J. M. Norman, and M. C. Anderson, "A simple and fast atmospheric correction for spaceborne remote sensing of surface temperature," *Remote Sens. Environ.*, vol. 87, no. 2/3, pp. 326–333, Oct. 2003.

[2] F. Jacob, A. Olioso, A. Gu, Z. Su, and B. Seguin, "Mapping surface fluxes using visible, near infrared, thermal infrared remote sensing data with a specialized surface energy balance model," *Agronomie*, vol. 22, pp. 669–680, Sep./Oct. 2002.

[3] E. F. Lambin and D. Ehrlich, "The surface temperature-vegetation index space for land cover and land-cover change analysis," *Int. J. Remote Sens.*, vol. 17, no. 3, pp. 463–487, Feb. 1996.

[4] C. J. Merchant and P. Le Borgne, "Retrieval of sea surface temperature from space, based on modeling of infrared radiative transfer: Capabilities and limitations," *J. Atmos. Ocean. Technol.*, vol. 21, no. 11, pp. 1734–1746, Nov. 2004.

[5] I. J. Barton, "Satellite-derived sea surface temperatures: Current status," *J. Geophys. Res.*, vol. 100, no. C5, pp. 8777–8790, May 1995.

[6] P. Y. Deschamps and T. Phulpin, "Atmospheric correction of infrared measurements of sea surface temperature using channels at 3.7, 11 and 12 μm," *Boundary-Layer Meteorol.*, vol. 18, no. 2, pp. 131–143, Mar. 1980.

[7] K. Matthew, C. M. Nagarani, and A. S. Kirankumar, "Split-window and multi-angle methods of sea surface temperature determination: An analysis," *Int. J. Remote Sens.*, vol. 22, no. 16, pp. 3237–3251, Nov. 2001.

[8] C. Prabhakara, G. Dalu, and V. G. Kunde, "Estimation of sea surface temperature from remote sensing in the 11–13 μm window range," *J. Geophys. Res.*, vol. 79, no. 33, pp. 5039–5044, Nov. 1974.

[9] F. Eugenio, J. Marcello, A. Hernandez-Guerra, and E. Rovaris, "Regional optimization of an atmospheric correction algorithm for the retrieval of sea surface temperature from the Canary Islands–Azores–Gibraltar area using NOAA/AVHRR data," *Int. J. Remote Sens.*, vol. 26, no. 9, pp. 1799–1814, May 2005.

[10] E. P. McClain, W. G. Pichel, and C. C. Walton, "Comparative performance of AVHRR-based multichannel sea surface temperatures," *J. Geophys. Res.*, vol. 90, no. C14, pp. 11 587–11 601, Nov. 1985.

[11] P. J. Minnett, "Radiometric measurements of the sea-surface skin temperature: The competing roles of the diurnal thermocline and the cool skin," *Int. J. Remote Sens.*, vol. 24, no. 24, pp. 5033–5047, Dec. 2003.

[12] S. J. Hook, F. J. Prata, R. E. Alley, A. Abtahi, R. C. Richards, S. G. Schladow, and S. O. Palmarsson, "Retrieval of lake bulk and skin temperatures using Along-Track Scanning Radiometer (ATSR-2) data: A case study using Lake Tahoe, California," *J. Atmos. Ocean. Technol.*, vol. 20, no. 4, pp. 534–548, Apr. 2003.

[13] M.-D. Chou, D. P. Kratz, and W. Ridgway, "Infrared radiation parameterizations in numerical climate models," *J. Clim.*, vol. 4, no. 4, pp. 424–437, Apr. 1991.

[14] I. Durre, R. S. Vose, and D. B. Wuertz, "Overview of the integrated global radiosonde archive," *J. Clim.*, vol. 19, no. 1, pp. 53–68, Jan. 2006.

[15] G. P. Anderson, J. H. Chetwynd, A. J. Ratkowski, G. W. Felde, J. A. Gardner, M. L. Hoke, B. Pukall, J. Mello, L. S. Jeong, and

A. Berk, "MODTRAN4—Radiative transfer for remote sensing," in *Proc. 6th Conf. Algorith. Multispectral, Hyperspectral, Ultraspectral Imagery*, Orlando, FL, Apr. 24–26, 2000, pp. 176–183.
[16] A. Berk, L. Bernstein, G. Anderson, P. Acharya, D. Robertson, J. Chetwynd, and S. Adler-Golden, "MODTRAN cloud and multiple scattering upgrades with application to AVIRIS," *Remote Sens. Environ.*, vol. 65, no. 3, pp. 367–375, Sep. 1998.
[17] F. Petitcolin and E. Vermote, "Land surface reflectance, emissivity and temperature from MODIS middle and thermal infrared data," *Remote Sens. Environ.*, vol. 83, no. 1/2, pp. 112–134, Nov. 2002.
[18] D. P. Kratz, "The correlated k-distribution technique as applied to the AVHRR channels," *J. Quant. Spectrosc. Radiat. Transfer*, vol. 53, no. 5, pp. 501–517, May 1995.
[19] F. M. Gottsche and F. Olesen, "Evolution of neural networks for radiative transfer calculations in the terrestrial infrared," *Remote Sens. Environ.*, vol. 80, no. 1, pp. 157–164, Apr. 2002.
[20] S. A. Clough, "The water vapor continuum and its role in remote sensing," *Opt. Remote Sens. Atmos.*, vol. 2, pp. 76–78, 1995.
[21] S. A. Clough, R. W. Davies, and R. H. Tipping, "The line shape for collisionally broadened molecular transitions: A quantum theory satisfying the fluctuation dissipation theorem," in *Proc. 6th Int. Conf. Spectral Line Shapes*, Boulder, CO, Jul. 12–16, 1982.
[22] W. B. Grant, "Water vapor absorption coefficients in the 8–13 m spectral region: A critical review," *Appl. Opt.*, vol. 29, no. 4, pp. 451–462, 1990.
[23] K. Y. A. Kondratiev, "Radiation in the atmosphere," in *International Geophysics Series*, vol. 12. New York: Academic, 1969, p. 911.
[24] D. R. Legates and G. J. McCabe, Jr., "Evaluating the use of 'goodness-of-fit' measures in hydrologic and hydroclimatic model validation," *Water Resour. Res.*, vol. 35, no. 1, pp. 233–241, 1999.
[25] S. J. Hook, R. G. Vaughan, H. Tonooka, and S. G. Schladow, "Absolute radiometric in-flight validation of mid infrared and thermal infrared data from ASTER and MODIS on the terra spacecraft using the Lake Tahoe, CA/NV, USA, automated validation site," *IEEE Trans. Geosci. Remote Sens.*, vol. 45, no. 6, pp. 1798–1807, Jun. 2007.
[26] I. J. Barton, P. J. Minnett, K. A. Maillet, C. J. Donlon, S. J. Hook, A. T. Jessup, and T. J. Nightingale, "The Miami2001 infrared radiometer calibration and intercomparison. Part II: Shipboard results," *J. Atmos. Ocean. Technol.*, vol. 21, no. 2, pp. 268–283, Feb. 2004.
[27] S. J. Hook, G. Chander, J. A. Barsi, R. E. Alley, A. Abtahi, F. D. Palluconi, B. L. Markham, R. C. Richards, S. G. Schladow, and D. L. Helder, "In-flight validation and recovery of water surface temperature with Landsat-5 thermal infrared data using an automated high-altitude lake validation site at Lake Tahoe," *IEEE Trans. Geosci. Remote Sens.*, vol. 42, no. 12, pp. 2767–2776, Dec. 2004.
[28] S. J. Hook, W. B. Clodius, L. Balick, R. E. Alley, A. Abtahi, R. C. Richards, and S. G. Schladow, "In-flight validation of mid- and thermal infrared data from the Multispectral Thermal Imager (MTI) using an automated high-altitude validation site at Lake Tahoe CA/NV, USA," *IEEE Trans. Geosci. Remote Sens.*, vol. 43, no. 9, pp. 1991–1999, Sep. 2005.
[29] H. Tonooka, F. D. Palluconi, S. J. Hook, and T. Matsunaga, "Vicarious calibration of ASTER thermal infrared bands," *IEEE Trans. Geosci. Remote Sens.*, vol. 43, no. 12, pp. 2733–2746, Dec. 2005.
[30] C. Coll, V. Caselles, J. M. Galve, E. Valor, R. Niclos, J. M. Sanchez, and R. Rivas, "Ground measurements for the validation of land surface temperatures derived from AATSR and MODIS data," *Remote Sens. Environ.*, vol. 97, no. 3, pp. 288–300, Aug. 2005.
[31] Z. Wan, Y. Zhang, Q. Zhang, and Z. Li, "Validation of the land-surface temperature products retrieved from Terra Moderate Resolution Imaging Spectroradiometer data," *Remote Sens. Environ.*, vol. 83, no. 1/2, pp. 163–180, Nov. 2002.

Evan Ellicott received the B.Sc. degree in environmental science and the B.A. degree in geography from The State University of New York, Albany. He is currently working toward the Ph.D. degree in the Department of Geography, University of Maryland, College Park.

He is currently a Research Assistant with the Department of Geography, University of Maryland. His research includes thermal atmospheric correction validation as well as investigations of fire radiative energy and associated biomass burning emissions.

Eric Vermote (M'95) received the Ph.D. degree in atmospheric optics from the University of Lille, Lille, France, in 1990.

He is currently a Senior Research Scientist with the Department of Geography, University of Maryland, College Park. His research interests cover radiative transfer modeling, vicarious calibration, atmospheric correction, and aerosol retrieval.

Dr. Vermote is a member of the Moderate Resolution Imaging Spectroradiometer Science Team, the NASA National Polar-orbiting Operational Environmental Satellite System Preparatory Project Science Team, and the Landsat Data Continuity Mission Science Team, and is responsible for the atmospheric correction over land surfaces in the visible-to-middle infrared.

François Petitcolin received the Engineering degree from the Ecole Nationale Superieur de Physique de Strasbourg, Strasbourg, France, in 1994 and the Ph.D. degree in environmental science and remote sensing from the University Louis Pasteur, Strasbourg, in 1999.

From 1999 to 2001, he was an Assistant Research Scientist with the University of Maryland, College Park, working with NASA Goddard Space Flight Center, Greenbelt, MD, on the first Moderate Resolution Imaging Spectroradiometer data. Since 2001, he has been with ACRI-ST company in France, where he leads the development of a prototype processor for the second ESA Earth Explorer Mission: SMOS.

Simon J. Hook received the B.Sc. degree from the University of Durham, Durham, U.K., in 1982, the M.Sc. degree from the University of Edmonton, Edmonton, Canada, in 1985, and the Ph.D. degree from the University of Durham in 1989.

He is a Principal Scientist with the NASA Jet Propulsion Laboratory, Pasadena, CA. He has been involved in the validation of several airborne and spacborne instruments including the Advanced Spaceborne Thermal Emission and Reflection Radiometer (ASTER), Landsat (5 and ETM+), the Moderate Resolution Imaging Spectroradiometer (MODIS), the MODIS/ASTER Airborne Simulator, the European Along Track Scanning Radiometers (ATSR2 and AATSR) and the Department of Energy's Multispectral Thermal Imager. His research is focused on improving our understanding of geologic and hydrodynamic processes.